UNIVERSITY
OF OULU

System For Measuring Steel Scrap Volume Using Depth Imaging

Abstract

Sustainability and green values are major themes in the world today. Companies across all fields are constantly implementing new technologies to reduce emissions and to limit the magnitude of global warming. The steel industry in general is one of the major producers of carbon dioxide emissions.

The objective of this thesis was to develop a system to measure the volume of scrap metal being charged to an electric arc furnace. Obtaining the scrap volume would help the furnace operators in timing the charging of scrap baskets, thus avoiding the adverse effects resulting from early and late charging. The intention is to increase the energy efficiency of the process.

The theory section of the thesis provides a short overview of the electric arc furnace process and a more detailed description of the charging process. Depth imaging technologies are then explored from a theoretical standpoint to provide the background for the selection and usage of imaging hardware.

In this thesis, design science research methodology was utilized to develop the scrap volume measurement system, which consists of imaging hardware and developed software. The actual contribution of this thesis is the algorithm to extract the height of the scrap surface level from a 3-dimensional image of scrap baskets. The development process was iteratively carried out in a steel factory.

The system performance was evaluated in a real-world scenario. It was established that the system was able to capture 3-dimensional data from scrap baskets and determine the scrap surface level height according to the algorithm. However, for some cases the image capturing did not perform as expected. These failure cases were a result of either steel dust obstructing the scene or the inability of the camera to capture data from unreflective material.

Further research prospects were identified during conducting of the thesis. The failure cases could be addressed either programmatically, with new hardware technology, or a combination of both. Also, research could be conducted on the usage of the information provided by the system in actual charging events with the goal of optimizing charging timing.

Foreword

This thesis is the finale of my studies in Information Processing Science in the University of Oulu and marks the decisive end of my time at the University, which admittedly has gone on for long enough. This and my previous Master's thesis for Process Engineering were both conducted during my time at Luxmet Oy. I have since moved on from the company to pursue a career in software development, but I wish to express my gratitude to Mr. Mikko Jokinen and Dr. Matti Aula for providing me this opportunity to further my studies while working in the company. I would also like to thank my thesis supervisor Dr. Pertti Seppänen for guidance.

Finally, a sincere thanks to my family and friends for support and positivity in everyday life. Especially Jenni and Rulla.

Tommi Veijola

Oulu, February 25, 2023

Abbreviations

API	Application Programming Interface
CW	Continuous Wave
DSR	Design Science Research
EAF	Electric Arc Furnace
FPFH	Fast Point Feature Histograms
GenICam	General Interface for Cameras
GigE	Gigabit Ethernet
HDR	High Dynamic Range
ICP	Iterative Closest Point
IOT	Internet Of Things
K-NN	K-Nearest Neighbours
LIDAR	Light Imaging Detection And Ranging
RMSE	Root-mean-square error
TOF	Time Of Flight
UDP	User Datagram Protocol
XML	Extensible Markup Language

Contents

1.   Introduction

Sustainability is a major topic of discussion in the world. To limit global warming, carbon dioxide emissions must be reduced. The challenge is great, and effects virtually every working sector.

Steel industry is a major producer of CO_2 emissions. According to the World Steel Association (2022), in 2021 1951 million tonnes of steel was produced in the world. Steel production has more than doubled in 20 years: in 2001 852 tonnes of crude steel was produced in the world. Each tonne of cast steel resulted in 1.89 tonnes of CO_2 emissions on average in 2020 (World Steel Association, 2021b). The steel industry was responsible for between 7 and 9 percent of global CO_2 emissions in 2020 (World Steel Association, 2021a). It has been estimated that in 2050 world steel production will grow to between 2500 Mt and 3000 Mt per year (Holappa, 2020).

Steel production can be roughly divided to ore-based and scrap-based production. Ore-based production is extremely energy demanding method and uses fossil fuels as the primary energy source. Scrap-based production is based on recycling steel and electric energy is used to melt the scrap metal. In 2021, 28.9 percent of steel was produced via the electric route (World Steel Association, 2022). Improving the energy efficiency of steelmaking reduces CO_2 emissions, thus contributing to limiting global warming.

With the introduction of numerous technological innovations, the manufacturing industry has seen major changes in the last decades. The cheap costs and miniaturization of smart sensors and other Internet of Things (IoT) devices accompanied by easy availability of high computing power has revolutionized production. This revolution is called the "Industry 4.0". The idea of Industry 4.0 is to integrate smart devices and other information and communication technologies (ICT) with conventional industries. Many such applications aim at improving the process by improving productivity and/or energy efficiency. (Cohen, Faccio, Pilati & Yao, 2019)

The development and use of depth imaging cameras has shifted from mainly research laboratories to commercially available products. The capability of cameras ranges from microns to a few kilometres (Sansoni, Trebeschi & Docchio, 2009). Combined with a decreasing cost and increased robustness, applying depth imaging sensors for industry and other applications has become reasonable. The applications range from surface quality control and micro profiling in the manufacturing industry to providing machine vision systems for robot applications (Sansoni et al., 2009). In the steel industry, automatic vision-based systems have been used for quality control. Recently, 3D measurements applications have become available to complement the traditional 2D imaging-based systems (Hao, Lu, Cheng, Li & Huang, 2021).

The objective of this thesis is to measure the volume of scrap metal being charged to an electric arc furnace (EAF). Obtaining the scrap volume enables the furnace operators to more accurately time the charging of the basket. The intention is to charge the basket as soon as possible to increase the energy efficiency of the process. 3-dimensional (3D) camera hardware will be used to capture a depth image of scrap baskets. A procedure will be formulated to obtain the scrap volume inside the basket by using the depth information provided by the camera.

The thesis is produced in cooperation with Luxmet Oy. Luxmet specializes in optical emission spectroscopy to measure online light intensity data from inside the furnace. The

scrap volume information is planned to be further used along with the Luxmet ArcSpec system to accurately time the scrap baskets to the furnace.

The thesis first describes the relevant background and theoretical basis for the relevant technologies: EAFs and depth imaging. The research method and implementation plan are then defined. The next two chapters cover the artifact design and development, which constitutes the practical part of the thesis. Next, the artifact performance is evaluated. The thesis results and implications are considered in the discussion chapter, followed finally by the conclusion.

2.   Background

The objective of this thesis is to develop a system for measuring the volume of scrap charge in the context of electric arc furnace steelmaking. 3D imaging hardware will be employed as measurement technology. Thus, relevant background information on electric arc furnaces and 3D imaging must be established. In this chapter, the relevant concepts, techniques, and technologies are explained to allow the reader to understand the rest of the thesis. First, a short summary of the EAF process is presented, along with a more detailed overview of the charging event and the influence it has on the rest of the process.

Next, an overview of the different depth imaging technologies is studied. Furthermore, time-of-flight (TOF) depth imaging is investigated in detail, along with the advantages and challenges associated with TOF imaging. Next, the types of data provided by depth cameras are shortly described. Finally, an overview of the relevant image processing methods is given.

2.1 Electric Arc Furnace Process

Electric arc furnaces are utilized in the steel industry to recycle scrap metal. An EAF is essentially a large metal structure in the shape of a cauldron, into which steel scrap is charged. Large graphite electrodes are then used to introduce electric energy into the scrap, forming an electric arc between the electrodes and the scrap.

The EAF process is generally operated as a batch process. A single EAF steel batch is called a heat. The EAF operating cycle is called a tap-to-tap cycle, which consists of the following operations: charging of the scrap metal, melting, refining, de-slagging, tapping, and turnaround. (Jones, Bowman & Lefrank, 1998)

The raw material for the EAF process is steel scrap. The scrap is stored in the scrap yard, where it is loaded into scrap baskets. There are numerous types of scrap in the scrap yard, depending on the rough chemical composition and the size of the scrap pieces. Oftentimes, the scrap contains contaminants, such as oil and dirt, which are undesirable in the process. The basket is loaded in a predetermined way to allow for fast melting and to achieve the desired chemical composition of the steel product. After loading, the scrap basket is transported to the EAF proximity on rails. The furnace roof and electrodes are moved out of the way and the basket is lifted on top of the furnace using a crane. Finally, the bottom of the basket is opened, allowing the scrap to fall into the furnace. (Jones et al. 1998)

After the emptied scrap basket is moved out of the way, the furnace roof and electrodes are moved back on top of the furnace. The melting stage is now ready to begin. The roof lowers to shut the furnace and the electrodes are lowered into the furnace through holes in the roof. As the electrodes contact the scrap, an electric circuit is formed, and electric arcs form between the electrodes and the scrap. This is the primary method of supplying energy into the scrap to melt it. Additionally, furnaces may employ burners or other devices to introduce chemical energy into the scrap by burning a mixture of natural gas and oxygen. Burners are commonly situated in the cold spots of the furnace, which are the areas located furthest away from the electrodes. If the heat consists of multiple scrap baskets, melting continues until the subsequent scrap charge fits into the furnace and the charging stage is repeated. After the final scrap charge is melted and flat bath conditions are reached, the melting stage is over, and refining may begin. (Jones et al. 1998)

The purpose of the refining stage is to achieve the desired chemical composition of the steel. Generally, this involves the removal of chemical components from the molten metal. The method of removing undesired components is allowing them to react with oxygen to form compounds which rise on top of the molten steel to form a layer called slag. The required oxygen is introduced into the furnace by blowing either through the furnace sidewall or from the bottom of the furnace. (Jones et al. 1998)

When the desired chemical composition and temperature of the molten steel is reached, the steel is recovered from the furnace. Before tapping, the slag layer from the top of the melt is removed. The slag is removed from the furnace by pouring it out through the slag door. Finally, the tapping stage may begin. The taphole is opened, and the molten steel is poured through it to a ladle by tilting the furnace. The ladle is a metal structure in the shape of a bucket that is used to transfer the molten steel. After the steel is recovered from the furnace, the turnaround operation may begin. In the turnaround stage, the furnace is prepared for the next batch of scrap to be melted. An inspection of the furnace insides is also carried out. (Jones et al. 1998)

The EAF is such a violent process that it is extremely difficult to obtain online data from inside the furnace. Therefore, the melting status of the scrap is instead inferred from measured process values that are related to melting. The melting process is inferred from, for example, the amount of electric energy and chemical energy introduced to the process during the melting process. This method of control is called static because it does not consider the dynamics of the process. Several characteristics of the EAF process introduce dynamic behaviour into the process, for example:

- the quality and composition of the steel scrap,
- how the scrap settles in the furnace,
- chemical reactions in the furnace, and
- slag formation.

2.1.1 Charging Event

Steel scrap is charged into an EAF using large metal baskets. The volume of the charged scrap is generally not known in advance to the furnace operators. It is a common practice that multiple scrap baskets are charged to the furnace during a single heat. The basket or baskets following the first basket should be charged as early as possible to maximize energy efficiency. The following presents three possible charging events, of which precisely one is desirable:

1. The scrap is charged too soon to the furnace, leading to an overcharge event.
2. The scrap is charged too late to the furnace, leading to lower energy efficiency.
3. The scrap is charged at the earliest moment when the new scrap fits to the furnace.

The overcharge event is undesirable, because it means that not all of the scrap was able to fit into the furnace. Therefore, the roof may not be able to close and the melting stage cannot begin. A practical solution is to use the charging basket to hammer the scrap until the roof may be lowered to its position.

Charging too late on the other hand means that the scrap will fit into the furnace with no problems. However, this event is also undesirable, as it leads to decreased energy efficiency, as well as reduced productivity. This is because as the melting stage progresses, the electric power supplied must be gradually decreased as the scrap melts to avoid damage to the furnace structure. In the early parts of melting, the electrodes bore

down into the scrap and the scrap shields the furnace walls from the intense radiation from the electric arcs. The efficiency of heat transfer decreases as a consequence of the scrap melting, as some of the heat is lost to the furnace walls and roof. Therefore, it is important to charge subsequent scrap baskets to the furnace at the earliest moment when there is enough room in the furnace.

2.2 Depth Imaging Technologies

According to Besl (1988), a range image is "a large collection of distance measurements from a known reference coordinate system to surface points on object(s) in a scene". Similarly, Hansard, Lee, Choi and Horaud (2013) note that depth images consist of pixels that contain the distance to the matching spot in the scene. Besl (1988) also defined range-imaging sensors as "any combination of hardware and software capable of producing a range image of a real-world scene".

Depth imaging is a wide topic where the researchers seem to use competing terminology when reporting their findings. For example, range finding (Jarvis, 1983), range imaging (Besl, 1988), three-dimensional shape measurement (Chen, Brown & Song, 2000), 3-D laser imaging (Blais, 2004) and 3D imaging (Sansoni et al., 2009) are some expressions that have been used by authors of notable surveys and reviews conducted on capturing range/depth information using optical sensors. Recently researchers seem to have shifted towards using terms such as "depth" and "depth imaging" (Hansard et al., 2013; Horaud, Hansard, Evangelidis & Ménier, 2016; Zanuttigh et al., 2016). This thesis will utilize the "depth" based terminology consistent with recent works. Moreover, there seems to be no general consensus on how specific depth imaging techniques and technologies are classified. This thesis follows the categorization of Sansoni et al. (2009) to aid in providing a concise overview of depth imaging technologies.

Sansoni et al. (2009) mention that there are a great number of varying optical techniques for depth imaging, and their classification is not straightforward. Nevertheless, the authors recognize that the techniques may be categorized into active and passive techniques. Active methods project electromagnetic energy onto an object, after which the reflected energy is received. Passive methods rely on recording electromagnetic energy from the object without actively projecting anything onto it. The authors also recognized the distinction between direct and indirect techniques. Direct techniques produce explicit range data, whereas indirect techniques produce data from which distance measurements may be inferred when combined with other information. Jarvis (1983) used similar terminology to categorize depth imaging techniques.

Besl (1988) noted four basic types of range sensors distinguished by their viewing constraints: point sensor, line or circle sensor, field of view sensor, and multiple view sensor system. A point sensor measures distance to a single point and to create a depth image either the measuring device, the measured object or both must be moved between subsequent measurements. Line sensors can measure multiple points at the same time along a line. Again, either the sensor or the object must be moved to create a full depth image. Field of view sensors can measure distances to each point in view of the sensor at once and thus does not require movement of the sensor or target to create a depth image. Multiple view sensor system consists of multiple sensors in cases where not all surface points or areas of interest can be made visible from a single viewpoint. (Besl 1988)

2.2.1 Time-of-flight depth imaging

Time-of-flight (TOF) depth imaging is an active technique for acquiring direct range data. This approach is based on the time interval a light pulse takes to travel from the camera to the target object and back (Jarvis 1983). The camera emits a pulse of light of a specific wavelength, some of which is reflected from the target object upon reaching it (Sansoni et al., 2009). The reflected pulse is received by a sensor in the camera, and the intensity and travel time of the signal is recorded (Sansoni et al., 2009). The simple equation for calculating distance is: (Besl 1988)

$$v\tau = 2r = \text{round-trip distance},\tag{1}$$

where v is the speed at which the signal travels, τ is the time interval between emitting and receiving the signal, and r is the distance to the target.

In a more recent review of specifically TOF technologies Horaud, Hansard, Evangelidis and Ménier (2016) use the term LIDAR (which stands for either "Light Imaging Detection And Ranging" or "LIght and raDAR") in parallel with TOF. They further detail that there are two different principles utilized for TOF: pulsed-light cameras (explained above) and continuous-wave (CW) modulated-light cameras. Pulsed-light cameras are further divided into scanning and scannerless types. Scanning cameras illuminate a single point or line at a time and thus must be equipped with functionality to rotate or otherwise adjust the angle of the emitted light to obtain the complete depth image. Scannerless cameras illuminate the entire scene at once and thus obtain the complete depth image at once. Continuous-wave modulation cameras determine distance indirectly by measuring the phase difference between the emitted and reflected signals, which is directly associated with distance. (Horaud et al., 2016)
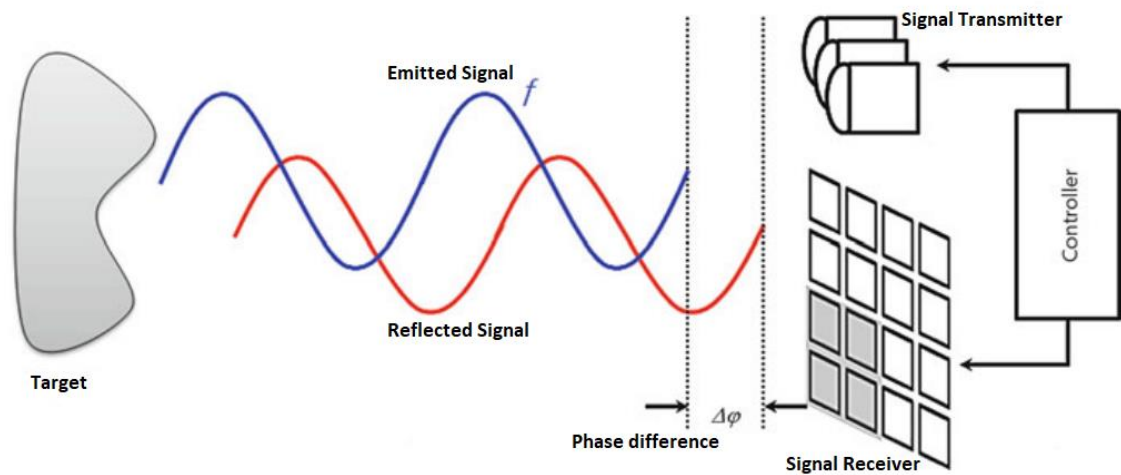
Figure 1. Operation of a continuous-wave modulated-light camera (Adapted from Hansard et al., 2013).

Figure 1 illustrates the operating principle of CW modulated-light cameras. The distance values can be calculated from (Hansard et al. 2013):

$$d = \frac{c}{2f}\frac{t_d}{2\pi}\tag{2}$$

where d is the distance to point in the scene, c is the speed of light, f is the frequency of the emitted signal and t_d is the measured phase difference.

2.2.2 Depth Camera Outputs

Depth imaging cameras produce multiple types of data. The most important construction is the point cloud, which is an unorganized set of (x, y, z) coordinate points that represent the target scene. Another common production is the amplitude image, which is associated with the amount of detected light signal per pixel (Lefloch et al, 2013). Lefloch et al. (2013) explain that the amplitude image may be used as a quality or reliability metric. Some cameras may also produce a confidence image as well as a grayscale 2D depth image.

(a) Amplitude image   (b) Confidence image

(c) Depth image   (d) Point cloud
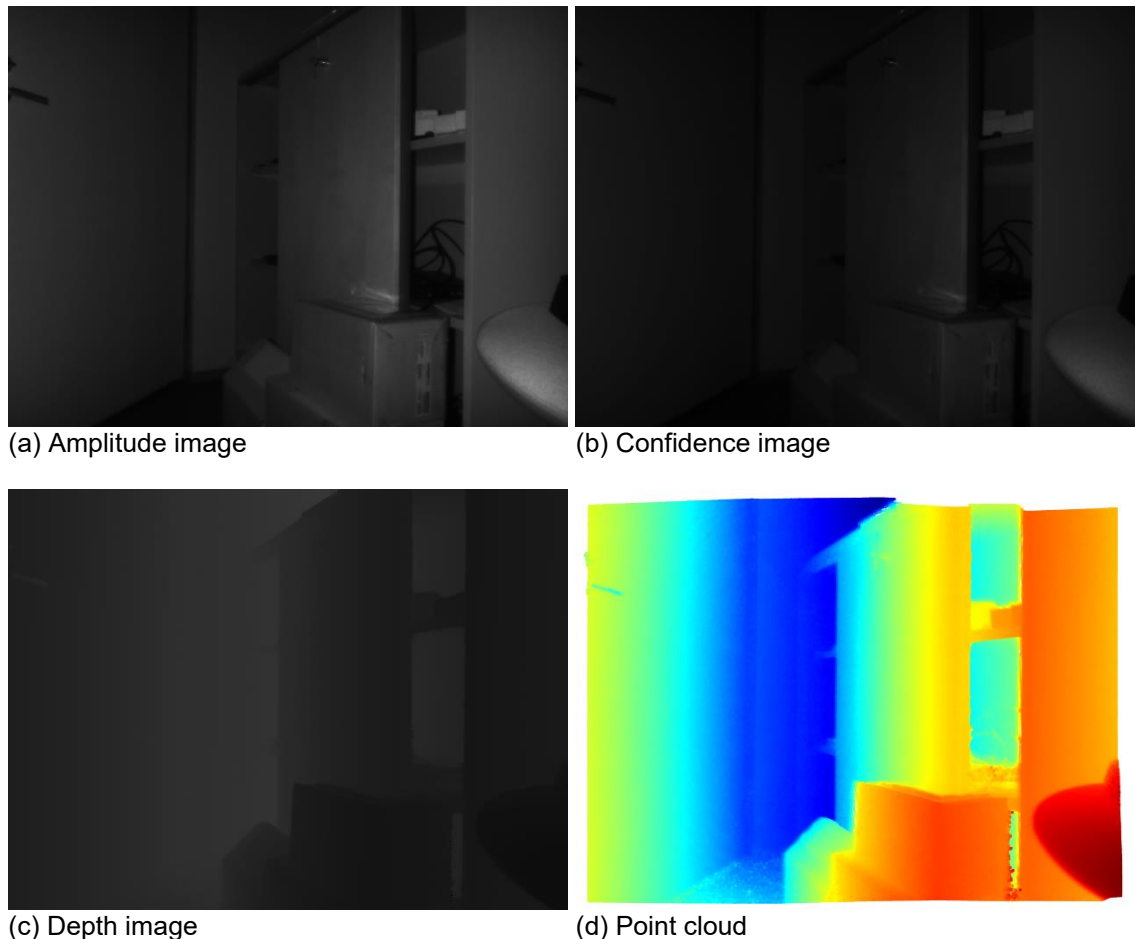
Figure 2. Example of depth camera outputs with 250ms exposure time.

Figure 2 presents example outputs from a TOF depth camera. The amplitude image (a) shows the intensity of the reflected light pulses. The second image (b) is the confidence image, which visualizes the reliability of captured depth data per pixel. A dark pixel corresponds to low confidence and a bright pixel corresponds to high confidence. The depth image (c) contains the captured raw depth data. The example image is in gray scale, with a darker pixel corresponding to a shorter distance and a brighter pixel to a farther distance. The final image (d) is the point cloud of the scene.

2.2.3 Depth Image Quality Considerations

Zanuttigh et al. (2016) provide a detailed analysis of possible issues with specifically TOF depth imaging. The first addressed issue, phase wrapping is an intrinsic issue of CW modulation cameras, as the wavelength of the signal directly limits the measurable distance. Another issue related to the sinusoidal nature of the signal used in modulation

cameras is harmonic distortion, meaning that it is difficult to create perfectly sinusoidal signals without distortion. Furthermore, recording the reflected signal has a similar issue, as the received signal is sampled in finite time intervals. This results in harmonic distortion and consequently in a predictable offset in measured distance. Lookup table correction is used to compensate for this offset. The next issue, photon-shot noise, is related to the dark electron current, which causes a disturbance in the receiver. (Zanuttigh et al., 2016)

(a) Amplitude image

(b) Confidence image

(c) Depth image

(d) Point cloud
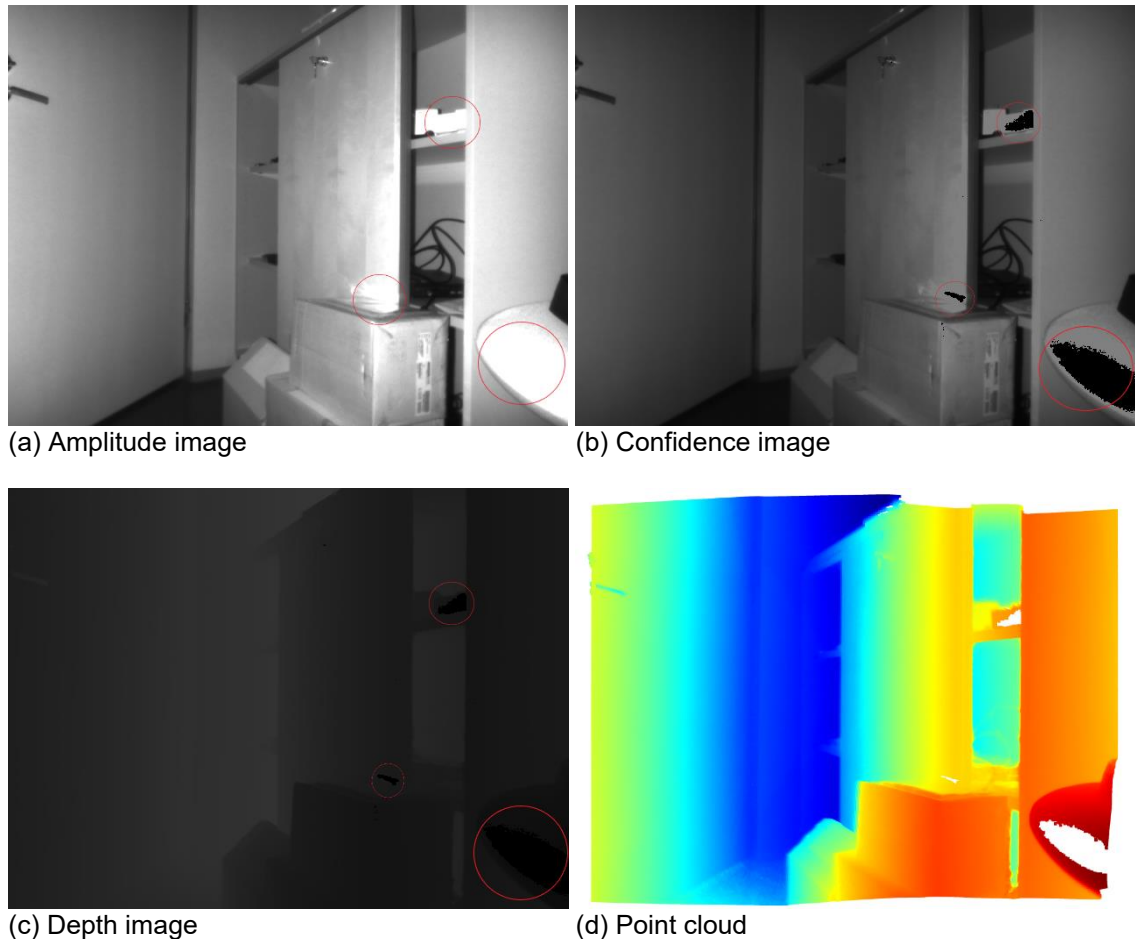
Figure 3. Example images captured using a TOF depth camera with 1000ms exposure time and saturated areas circled in red.

Averaging measurements over time is effective in reducing noise from the measurement. However, averaging presents the issues of saturation and motion blur. Saturation happens when the number of photons received exceeds the amount the receiver can handle. Saturation is more common when there is a source or reflection of uncontrolled IR radiation present in the scene or if there are highly reflective surfaces in the scene. Figure 3 presents example images of a scene where saturation was experienced. The image was captured using a TOF depth camera. The very brightest spots in the amplitude image (a) are black in the confidence image (b) and depth image (c). The corresponding pixels in the point cloud (d) are white, indicating no measurement. The saturated areas are circled in red for illustration purposes.

Motion blur occurs when objects in the scene move during the averaging period. The effect is comparable to that of normal cameras. The averaging (or integration) time may be adjusted to compensate for these. It should be noted that tuning the averaging time is a compromise between allowing for noise in the measurement and mitigating saturation and motion blur. (Zanuttigh et al., 2016)

(a) Amplitude image

(a) Point cloud (front view)

(a) Point cloud (right side view)

(a) Point cloud (top view)
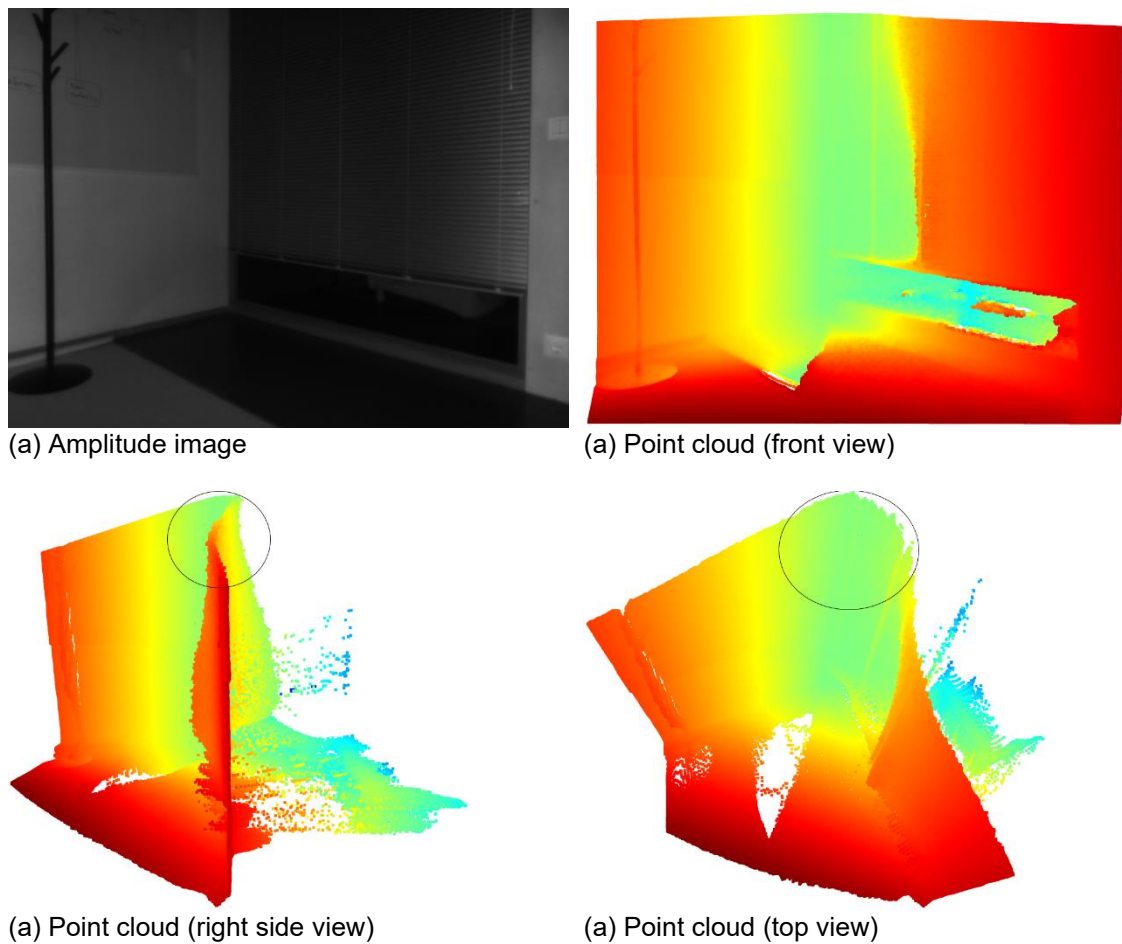
Figure 4. Example depth camera outputs with a reflective scene.

Ideally, projected light is reflected back from the target in a single beam. However, in reality this is not the case due to scattering of the light when hitting the target. Some of the scattered light may be observed by the sensor after multiple reflections, resulting in what is referred to as multipath error. Most of the time the magnitude of the primary reflection outweighs the energy compared to the secondary reflections. Figure 4 presents a scene with reflective surfaces. Notice that the corner (circled in black) does not appear sharp in the point clouds but appears rounded. This rounding is the result of a multipath error due to the emitted light reflecting multiple times between surfaces.
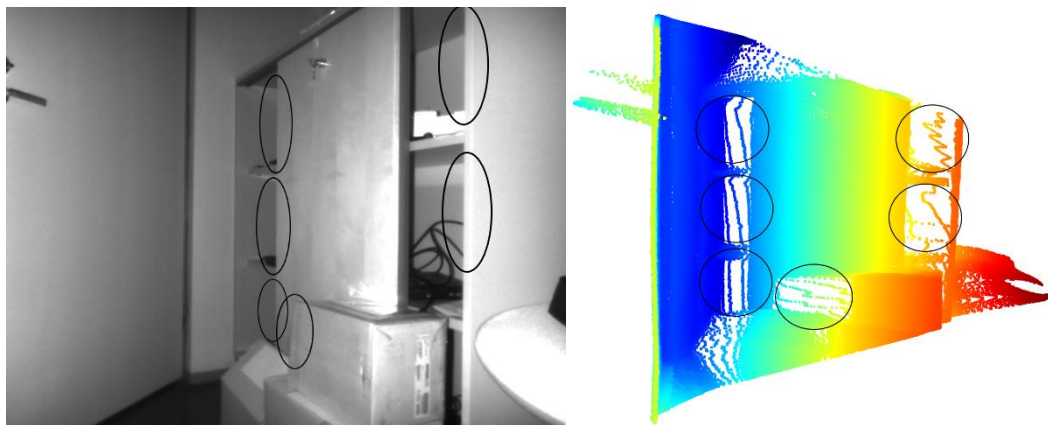
Figure 5. Example of depth camera outputs with flying pixels present. Left image shows the amplitude image, and the right image is the point cloud (left side view). The areas circled in black point to corresponding areas between the images.

Another problem similar to multipath error is the problem of flying pixels, which is a result of the pixel size in the sensor. Each pixel corresponds to a small region in the target scene. If there are sharp changes of depth in the region the distance may be incorrectly estimated because the combination of the signals is inconsistent. Figure 5 illustrates example depth camera outputs containing flying pixels. Note the areas circled in black in the amplitude image: these are areas with sudden changes in depth. Flying pixels appear in the corresponding areas in the point cloud. This effect could be mitigated by calculating a confidence value for pixels based on the intensity and amplitude of the observed signal. (Zanuttigh et al., 2016)

2.2.4 Point Cloud Filtering

In the context of outlier identification, multiple studies (Knorr & Ng, 1998; Breunig, Kriegel, Ng & Sander, 2000; Sugiyama & Borgwardt, 2013) cite the outlier definition by Hawkins (1980): "An outlier is an observation that deviates so much from other observations as to arouse suspicion that it was generated by a different mechanism." As explained above, time-of-flight cameras suffer from several intrinsic and extrinsic error sources. The erroneous measurements arising from error sources related to the scene and the environment may be identified as outliers as per the above definition by Hawkins. The objective of depth image filtering is to remove outliers, such as erroneous measurements (Axelsson, 1999). Further processing of point clouds necessitates the filtering of these outliers (Han et al., 2017).

Nurunnabi, West and Belton (2015) point out that detecting outliers in point cloud data is difficult because of the disorganized, noisy, and ambiguous nature of the data. According to Han et al. (2017) methods for filtering point clouds may be categorized into seven groups: statistical-based filtering, neighbourhood-based filtering, projection-based filtering, signal processing-based filtering, PDEs-based filtering, hybrid filtering, and other methods. They further provide a review on algorithms for each category.

Rusu, Marton, Blodow, Dolha & Beetz (2008b) employed a simple outlier removal method with good results. The method first calculates the k-nearest neighbours (K-NN) distances for all measurement points. Subsequently, the mean and standard deviation of the calculated distances are determined. Finally, points that have a K-NN distance outside the following range are removed (Rusu et al, 2008b):

$$\mu \pm \alpha \cdot \sigma, \tag{3}$$

where μ is the mean and σ is the standard deviation of the K-NN distances, and α is a scalar that signifies the magnitude of filtering (greater number results in fewer points removed). The authors used values $\alpha = 1$, and $k = 30$ (for the K-NN algorithm). The value of α indicates how much the K-NN value of a point may differ from the mean before it is considered an outlier. If the distances were normally distributed, an α value of 1 would filter out about 32% of the points. However, Rusu et al. (2008b) report that roughly 1% of the points were filtered using the stated values. (Rusu et al., 2008b)

2.2.5 Point Cloud Pairwise Registration

Registration of point clouds refers to the process of aligning two or more point clouds with each other (Rusu, Blodow & Beetz, 2009). The objective of registration is to find the transformation operations that when applied to a source point cloud, overlaps it with

a target point cloud (Chen & Medioni, 1991). The problem of finding such a transformation is called the correspondence problem, in other words which points in the source point cloud correspond with which points in the target point cloud (Chen & Medioni, 1991). The problem manifests itself in numerous ways: building a digital model from a physical object (Chen & Medioni, 1991), measuring the similarity of a physical object and a model of said object (Besl & McKay, 1992), and obtaining 3D object maps of rooms (Rusu et al, 2008b) to name a few. Point cloud registration is commonly performed in two steps: a rough alignment, followed by a more refined alignment (Zanuttigh et al., 2016).

The objective of the rough registration is to find an initial transformation as an input to the fine registration (Rusu, Blodow, Marton & Beetz, 2008a). In their paper on efficient variants of the IPC algorithm, Rusinkiewicz & Levoy (2001) mention some methods for finding a rough alignment, among them surface feature identification and indexing, and manual transformation. Clearly manual finding of a rough transformation is out of the question for any actual application of point cloud registration. Rusu et al. (2008a) presented a method for calculating explanatory feature values, such as whether the point belong on a plane or some other geometric shape, for point cloud data. The authors called their construction "persistent point feature histograms". They demonstrated that when combined with an alignment algorithm based on geometric features, the method proved superior to other methods. Later, Rusu et al. (2009) improved on the work by Rusu et al. (2008a) into a more optimized version called "fast point feature histograms" (FPFH). Zhou, Park & Koltun (2016) presented an algorithm for "fast global registration" to compute very quickly an excellent initial transformation. As the feature set in the algorithm, they used the FPFH presented by Rusu et al. (2009).

Fine registration uses the initial transformation as a starting point to find a transformation that aligns the point clouds tightly. The algorithm used for this step is usually some variant of the iterative closest point (ICP) algorithm (Zanuttigh et al., 2016). ICP algorithms necessarily converge to a local minimum (Chen & Medioni, 1991; Besl & McKay, 1992). In their paper introducing the ICP algorithm, Chen & Medioni (1991) explain that the algorithm does not necessarily ensure that the global minimum is found due its iterative nature. The authors therefore argue that a good initial guess is vital. The rough registration explained above is precisely the solution for obtaining such a guess. Rusinkiwicz & Levoy (2001) reviewed and evaluated some ICP algorithms, while also presenting an optimized ICP algorithm.

2.3 Depth Imaging Applications in Steel Industry

Depth imaging has been utilized in the steel industry mainly as a means for online quality control of steel products. Traditionally, surface quality inspection of steel products are laborious tasks. Such methods include cutting a sample of the product to be inspected by an expert or stationing process operators on the product line to inspect the product for any defects (Neogi, Mohanta & Dutta, 2014). Automated vision-based systems have been applied in steel surface defect inspection as a more effective solution. According to Neogi, Mohanta & Dutta (2014), the most noteworthy categories of steel surfaces inspected for defects are slab, billet, plate, hot strip, cold strip, and rod. Slabs and billets are semi-finished products that are produced directly from liquid steel by the continuous casting process. Plates and hot strips are produced from slabs after reheating and rolling to desired thickness. The surface of these products is oxidized. Cold strips may be further produced from hot strips in cold rolling mills. Rods are produced from billets by a hot rolling process. There is no general consensus on the categorization of defects in the steel

products, but the most noteworthy defects are different types of cracks. The defects are a result of flawed casting and the huge forces used in the rolling processes. (Neogi, Mohanta & Dutta, 2014)

Conventional cameras are commonly used to capture images of the steel surface. However, such systems suffer from pseudo-defects, which are non-defects with features like actual defects, caused by inconsistent lighting conditions (Landström & Thurley, 2012). As an improved solution to steel surface defect monitoring, Landström & Thurley (2012) proposed the use of depth imaging to detect imperfections on steel surfaces more reliably. Their system used 3D profile data of steel slab surfaces to detect cracks and was based on morphological image processing and statistical classification. Zhao, Ouyang, Chen & Wen (2011) described a 3D inspection method to find defects on continuously cast slab surface. Park, Bae, Yun & Yun (2013) also developed a hot slab surface inspection system based on depth imaging. Hsu et al. (2017) described a 3D modelling framework for capturing 3D data from steel billet images. Hsu et al. (2018) introduced an automatic steel product tracking system based on 3D data features, contrary to the normal practice of embedding an identification code on the steel surface.

3.   Research Method

This thesis follows the methodology for conducting design science research (DSR) presented by Peffers, Tuunanen, Rothenberger & Chatterjee (2007). According to Hevner, March, Park & Ram (2004), DSR is a research paradigm intended for problem solving. Hevner et al. (2004) continue that the objective of DSR is to construct innovative artifacts that "define the ideas, practices, technical capabilities, and products through which the analysis, design, implementation, management, and use of information systems can be effectively and efficiently accomplished." Another definition provided by Hevner et al. (2004) states that DSR constructs and critically assesses Information Technology (IT) inventions aimed at solving specific problems found in the industry. Peffers et al (2007) distinguish design science from other paradigms by citing Simon (1969): "Whereas natural sciences and social sciences try to understand reality, design science attempts to create things that serve human purposes". In this chapter, the DSR methodology presented by Peffers et al. (2007) is explored. Each research activity is investigated and explained. Finally, the research questions guiding this thesis are given and the implementation of the methodology to answer them is described.

3.1 Design Science Research Methodology

Hevner et al. (2004) described seven guidelines for conducting design science research:

1. research must produce an artifact,
2. the artifact must solve a meaningful business problem,
3. the applicability and performance of the artifact must be evaluated,
4. the research provides real a contribution to its respective field,
5. artifact construction and evaluation must be executed in a meticulous manner,
6. existing expertise must be utilized in the design of the artifact, and
7. the research must be communicated to relevant audiences.

According to Peffers et al. (2007), a complete methodology consists of three components: *principles* (definition), *practice rules* (the guidelines by Hevner et al., 2004) and finally a detailed *procedure* as how to execute the research. Peffers et al. (2007) formulated the missing *procedure* component to complement the prior work of others and thus developed a complete methodology for design science in information systems. Peffers et al. (2007) attempted to identify elements of research that had been generally established as appropriate in the field. They used seven papers as basis for discovering process elements associated with the DSRM process. Figure 6 presents the procedure in a visual form. The procedure is designed to be iterative after the problem definition.
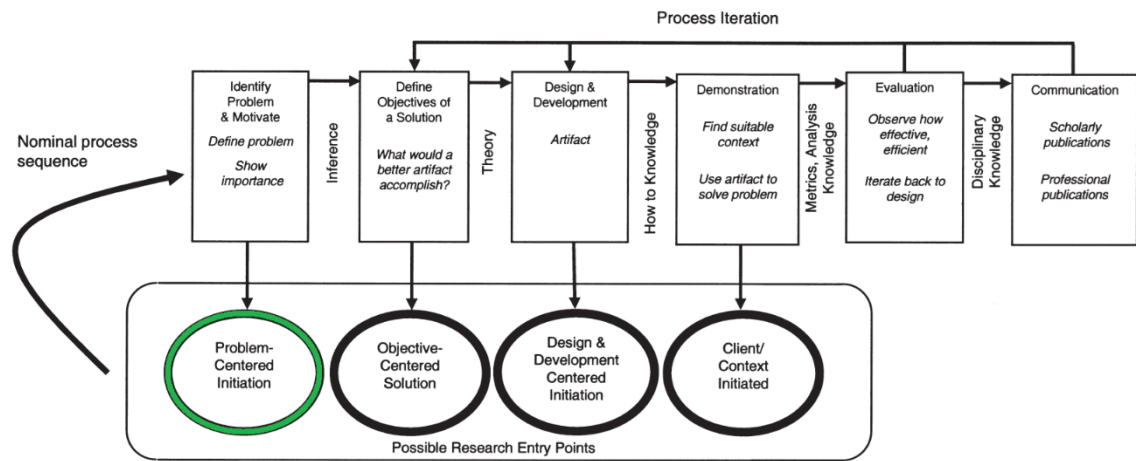
Figure 6. DSR Process (adapted from Peffers et al., 2007)

The procedure presented by Peffers et al. (2007) is as follows:

1. definition and justification of the problem,
2. definition of the goals for a solution,
3. design and development of the artifact,
4. demonstration of the applicability of the artifact to solve the problem,
5. evaluation of the performance of the artifact, and
6. communication of the research.

3.1.1 Problem Definition and Motivation

Peffers et al. (2007) synthesised the definition of the problem as the first activity in the methodology. This activity also contains reasoning what a solution would accomplish and what value it would bring in the scope of the problem. Peffers et al. (2007) further argue that breaking down the problem into detailed parts is beneficial for crafting an artifact that solves the problem, as this helps the designer capture the intricacies of the problem. Establishing the hypothetical value of solving the problem provides the researcher and the target audience with inspiration to focus efforts on solving the problem. Furthermore, it helps with conveying the reasoning behind why the research must be carried out. Finally, Peffers et al. (2007) communicate the resources required for this activity, which are expertise of the problem in its respective context and the significance of its solution.

3.1.2 Objectives of the Solution

The second activity identified by Peffers et al. (2007) is defining what objectives the solution must accomplish. The objectives should be derived from the problem definition considering what is achievable and reasonable. The objectives can be formulated in different ways according to the nature and context of the problem. One possibility is to describe what benefits the solution should offer compared to existing ones. This activity requires expertise on the problem, what existing solutions there are, how effective they are, and what room for improvement there is. (Peffers et al. 2007)

3.1.3 Artifact Design and Development

The artifact is created in this activity. According to Peffers et al. (2007), an artifact can be any designed object that incorporates the research contribution in its design. In this activity, the range of capabilities of the artifact are decided according to the objectives the artifact must accomplish. Furthermore, the architecture of the artifact is developed, and the actual artifact created accordingly. Expertise on the theory related to the artifact instantiation is required in this activity. (Peffers et al. 2007)

3.1.4 Applicability Demonstration

In this activity, the applicability of the artifact to solve the problem is demonstrated. The artifact should be employed in the problem context as a means for solving the problem. This could be performed for example in a simulation, case study, experiment, or other such endeavour. This activity requires expertise on how the artifact should be used to solve the problem. (Peffers et al. 2007)

3.1.5 Performance Evaluation

This activity includes evaluating the performance of the artifact in solving the problem. Depending on the context, this could involve for example observing and measuring how the artifact performs in solving the problem. Additionally, the observed outcome should be compared to the objectives of the artifact defined previously in activity 2 (Objectives of the Solution). Finally, the researcher considers whether to return to activity 3 (Artifact Design and Development) to improve on the artifact or not, based on the performance of the artifact. It is also possible to leave further improvements to future projects. (Peffers et al. 2007)

3.1.6 Research Communication

The final activity is communicating the consequences and implications of the research to target audiences. Peffers et al. (2007) suggest that researchers could use the structure of the DSMR process as the structure for research papers.

3.2 Methodology Implementation

The purpose of the thesis is to develop a system for measuring the fullness of scrap baskets loaded to electric arc furnaces. The research entry point is Problem-Centered Initiation, circled in green in Figure 6. The following research questions are formulated to provide direction for the thesis.

1. *How can scrap volume information be extracted from a Point Cloud captured of a scrap basket?*

    a. *How does image quality influence the outcome?*

    b. *What other factors influence the outcome?*

This thesis seeks answers to these questions by employing the design science research methodology.

Problem Definition and Motivation

As explained earlier, several scrap baskets may be charged into an EAF during a single heat. It is beneficial to accurately time the charging to prevent undesired events. Accurate timing of the charging event requires information on the following properties:

1. The melting status of the scrap inside the furnace.
2. The volume of the scrap basket to be charged.

As discussed before, neither of these properties are generally known to the operators before the actual charging event. The furnace operators must make decisions based on inferred and incomplete data, which increases the risk of inaccurate charge timing.

The critical question is: "Does the next charge fit into the furnace?". This question may also be formulated as: "Is the free volume in the furnace greater than or equal to the volume of the scrap charge?". To answer this question, two sub-questions are derived: "What is the free volume in the furnace?", and "What is the volume of the scrap charge?". This thesis focuses on the latter question.

As discussed earlier, obtaining accurate information on the volume of the scrap charge leads to a more accurate charging timing, which results in improved process efficiency and productivity. A solution to this problem would provide accurate volume information to the operators and the automation system to enable more accurate charging timing.

Objectives of the Solution

The naïve solution involves estimating the volume of the scrap in the baskets after the first basket visually by the operators. This solution has multiple issues, however. Visually estimating the scrap volume requires operators to be able to see the basket. There are two alternatives for accomplishing this: visually inspecting the basket by walking over to the waiting scrap basket or using cameras to see the basket. Depending on the factory safety regulations, entering the furnace area when the furnace is powered might be forbidden due to safety concerns. Cameras might solve this problem, but it will not eliminate the human error from the volume estimation. Further, different people will have different estimates on the volume.

The objective of the solution researched in this thesis is to obtain accurate scrap volume information from the charging basket in an autonomous manner and relay this information to the operators and the automation system, eliminating the human factor completely.

Artifact Design and Development

The artifact to be designed and developed in this thesis is a system that accomplishes the following:

1. obtain signal when the scrap basket is in position,
2. use imaging hardware to capture a point cloud of the scrap basket,
3. calculate scrap volume using the data in the point cloud, and

4. relay the volume information to furnace operators and automation system.

The system consists of both hardware and software. The hardware used is a 3D camera to capture a point cloud image of the scrap basket and a computer. Software will be developed to communicate with the factory automation system and capture images from the 3D camera. An algorithm or procedure will be designed and developed to extract volume information from the captured images. The algorithm or procedure will be implemented in software.

Applicability Demonstration

The applicability of the artifact will be demonstrated in a factory environment by experimenting with using the system. Demonstration will include receiving basket location signal from the automation system, capturing a point cloud image of the scrap basket and successfully calculating the scrap volume information using the developed algorithm.

Performance Evaluation

The performance evaluation of the system focuses on the ability and efficiency of the system to calculate the volume of the scrap charge. Some properties to consider are the quality of the image captured by the 3D camera, the accuracy of the camera, the speed of the image capturing, computation speed of the algorithm and the algorithms robustness to disturbances in the image. The critical property obviously is the accuracy of the scrap volume measurement. However, verifying the accuracy is not trivial, because it is very likely that there is no way to determine the actual volume of the scrap charge to compare the result against. One possibility is to compare a set of captured images and calculated volumes and comparing them against each other to see if the algorithm is consistent.

Research Communication

This thesis serves as the communication medium for the research.

4.   Artifact Design

This chapter discusses the imaging environment and the hardware that will be used for capturing images of scrap baskets in a steel factory. The imaging environment is static, and the camera will be placed on a railing in an angle compared to the basket. The hardware used for capturing the images is the Blaze-101 camera from Basler, which uses Time-of-Flight measuring method to capture a depth image of the full scene at once. The chapter discusses the various physical interfaces of the camera and the protocols used for communication between the camera and the PC. Furthermore, various image quality features of the camera are presented. A short overview of the software design is given. Finally, the algorithm design is explained.

4.1 Imaging Environment

The environment where imaging will take place is a steel factory. Scrap baskets arrive to the loading zone on a carriage riding on rails. Figure 7 presents the plan for the imaging environment. The baskets always stop in the same place below a crane, which is used to lift the basket and transport it over the open furnace. In Figure 7, note the proposed placement of the camera. There is a walking platform next to the loading zone with clear view to the basket. Optimally, the camera would be situated perpendicular to the scrap basket. However, that is not possible in this case. The camera will therefore be placed on a railing in some angle compared to the basket. It is noteworthy that the camera placement, camera angle relative to the basket, and the basket position are static between captured images.
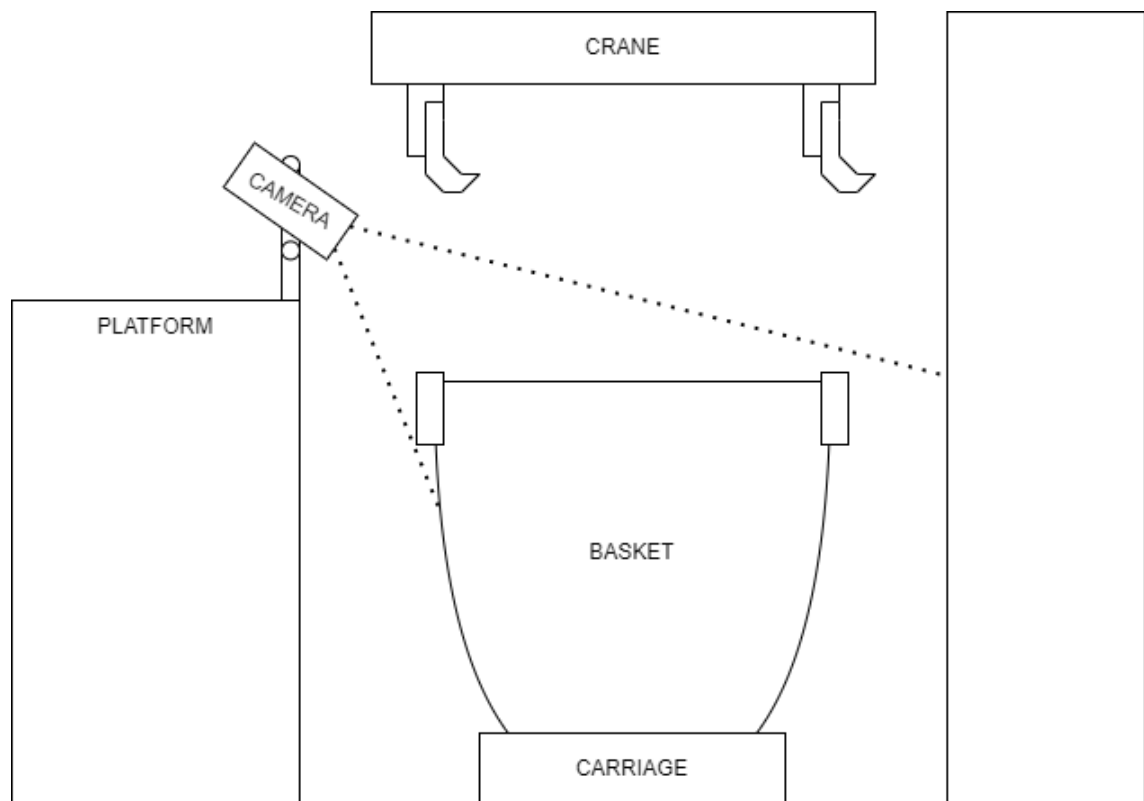
Figure 7. Imaging environment.

4.2 Hardware

The camera used for capturing images of the basket will be the Blaze-101 model from manufacturer Basler. The measuring method is Time-of-Flight, and the actual sensor is the Sony DepthSense IMX556. The bulky design of the camera allows for a wide range of custom installation options. Time-of-Flight measurement method is selected to capture a depth image of the full scene at once, without the need for physically moving the camera or the target object. This simplifies the implementation of image capturing. The camera model is selected based on retailer availability, price, ethernet data interface, camera features, such as different filtering mechanisms, and resilience to harsh environments. Figure 8 shows an image of the camera.

Figure 8. Basler Blaze-101 camera.

The camera has two physical connectors: data and power. The data connector is a M12, 8-pin, x-coded, female ethernet connector. The power connector is a M12, 8-pin, female connector. The physical interfaces are shown in Figure 9.

Figure 9. Basler Blaze-101 physical interfaces.

All communication between the PC and the camera is accomplished according to protocols specified in the GigE Vision standard: GigE Vision control protocol, GigE Vision stream protocol, and GigE device discovery protocol. The protocols employ the User Datagram Protocol (UDP) for data transfer. GigE Vision is a proprietary standard, of which Basler provides an implementation along with their camera. In addition to the mentioned protocols, an Extensible Markup Language (XML) file describing camera-specific details is required. The camera conforms to the Generic Interface for Cameras (GenICam) application programming interface (API), which enables configuring and operating cameras using a uniform programming interface, regardless of the underlying transport layer interface used to communicate with the camera. The camera manufacturer delivers a description file according to the GenICam standard. The file maps configuration nodes to registers on the physical camera, as well as implements the transport layer interface.

The Basler Blaze-101 depth camera contains numerous features that may be configured as necessary using the GenICam API. There are no definitive guidelines for selecting and manipulating features, as they depend on the properties of the imaged scene. Features that aim to remove incorrect measurements may be enabled and disabled. Many such features may be additionally configured through a threshold or strength value. There are also features such as region of interest, exposure time and pixel formats, to name a few (Basler, 2022).

4.2.1 Image Quality Features

The camera internally implements the following image quality features: ambiguity filter, confidence threshold, outlier removal, spatial filter, and temporal filter. The ambiguity filter, as the name states, removes ambiguities from the depth calculation. It aims to solve the issue of phase wrapping, which was explained earlier in this study. There is also a threshold value that may be used to adjust the strength of the filtering. This threshold value is a compromise of detecting ambiguities and removing correct distance measurements.

Next, for every pixel the camera calculates a confidence value that signifies the reliability of the distance measurement for that pixel. It is calculated from the amount of light collected for that pixel. A threshold value may be chosen to filter measurements with a low confidence value. This value should be determined empirically for each imaging scene.

Outlier removal is a feature that attempts to remove pixels that differ significantly from their neighbourhood. The camera uses an internal algorithm to calculate this. For this feature, there is again a threshold value that may be used to adjust the strength of this filter. Pixels that are deemed outliers are removed from the final depth image. Again, there is no conclusive guideline on selecting the threshold value. It must be determined individually according to the scene environment.

The spatial filter aims at smoothing out surfaces in depth images by removing spatial noise from the measurement. This filter may only be enabled or disabled, there is no strength value to adjust.

The temporal filter attempts to filter out temporal noise from the measurement. The filter operates using information from multiple frames. The objective is to remove motion artifacts, which as explained before is a result of averaging distance measurements using multiple frames. The filter analyses pixels between frames and tries to detect whether the distance measurement for pixels differ significantly between frames. There is a strength value that may be adjusted to control the filtering.

4.2.2 Other Features

Other notable features of the camera that may be adjusted are minimum and maximum range of measurement, the exposure time, and the pixel formats of the camera. The minimum and maximum range are self-explanatory, they are used to define the region of interest. The exposure time is an important parameter that may have a great effect on the measurement. Generally, the exposure time should be set as maximum possible and then lowered as necessary if there are highly reflective elements in the scene that result in saturation. The pixel formats are useful in selecting how the images are represented in data. The camera allows capturing depth images, intensity images, confidence images and point clouds. For each, the pixel format may or may not be adjustable.

4.3 Software

Software will be developed to configure and operate the camera. Additionally, the algorithm for extracting the scrap volume from the captured point cloud will be developed and implemented in software. The software will be written in Python programming language to enable rapid development. Furthermore, the author is well familiar with Python and the availability of useful libraries for Python is excellent.
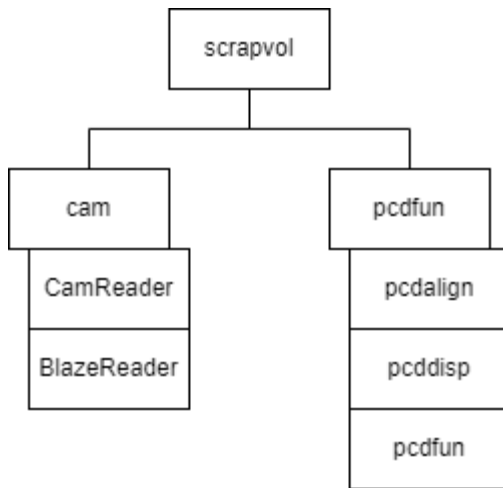
Figure 10. Scrapvol python package hierarchy.

The design for the *scrapvol* python package is presented in Figure 10. The *cam* module will contain the components related to configuring and operating the camera, whereas the *pcdfun* module will contain components related to manipulating the captured point clouds and implementing the algorithm for obtaining the volume of the scrap.

In addition to configuring and operating the camera, software will be developed to communicate with the factory automation system. The purpose is to receive signals whenever a scrap basket arrives at the loading zone and subsequently transmitting the calculated scrap volume to the automation system.

4.4 Scrap Volume Algorithm

The algorithm to obtain the scrap volume will exploit the fact that the camera placement and the scrap basket position is static. Therefore, it is safe to assume that the captured images will be roughly similar in what portion of the basket is visible to the camera. The first objective of the algorithm is finding the basket top edge, which in combination with knowledge of the basket depth will be used to calculate the volume later. Second, a coordinate transform will be performed on the point cloud to shift the z-axis (corresponding to the distance) to be perpendicular to the basket edge. Figure 11 illustrates the coordinate transformation. The objective of the transformation is to obtain distance values that are directly comparable between one another. Moreover, the z-coordinates of the pixels will directly relate to height after the transformation. Finally, all the image pixels of the scrap surface must be found. The scrap surface will most likely not be smooth, so an average value of the height of the pixels must be found. Figure 12 presents the information obtainable after transformation and finding the basket edge and scrap surface pixels.
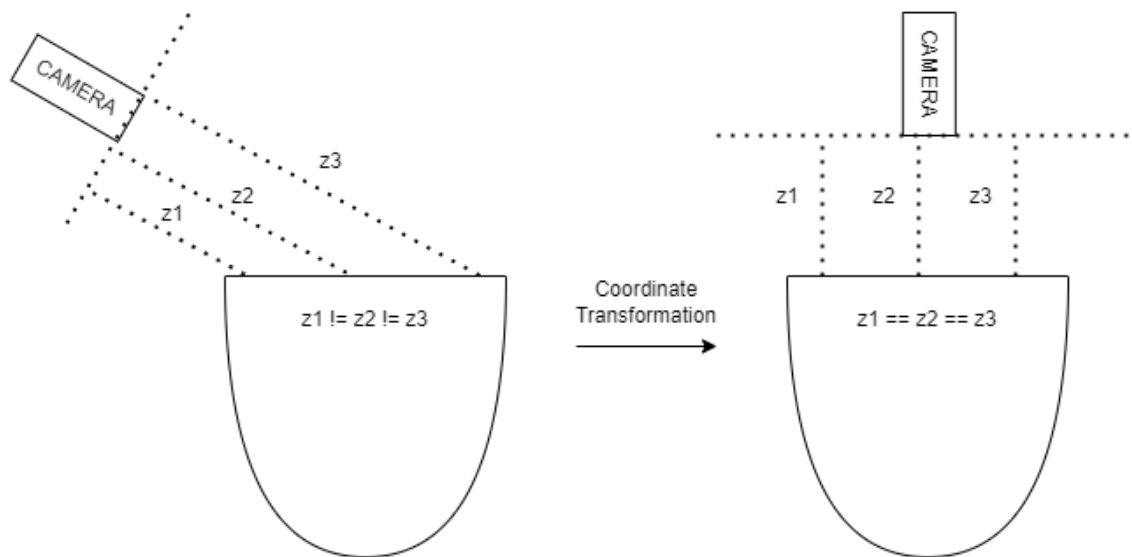
Figure 11. Coordinate transformation.
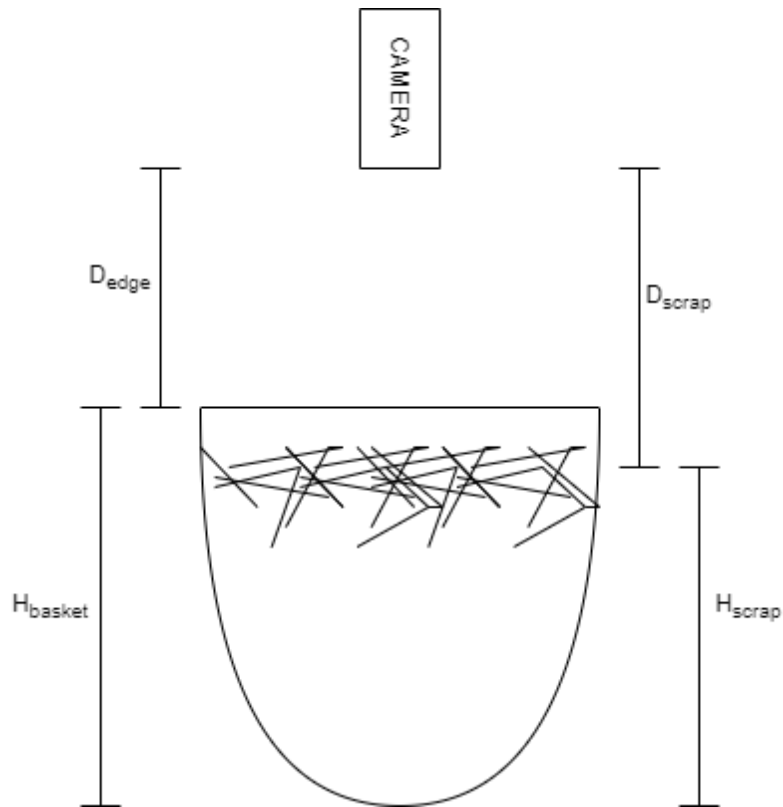
Figure 12. Scrap basket height calculation.

After the transformation and finding the distances to the basket top edge and scrap surface, the height of the scrap surface relative to the basket may be calculated using the equation:

$$H_{scrap} = H_{basket} + D_{edge} - D_{scrap}, \tag{4}$$

where H_{scrap} is the height of the scrap surface from the bottom of the basket, H_{basket} is the height of the scrap basket, D_{edge} is the distance from the camera to the basket edge, and D_{scrap} is the average distance from the camera to the scrap surface. Thereafter, the fill percentage of the basket may be calculated by dividing the scrap height with the basket height.

5.   Artifact Development

This chapter presents detailed information on the implementation of the camera system to capture images of scrap baskets, and the algorithm to extract scrap volume data from the captured images. First, the installation location and orientation of the camera are explained. Encountered issues related to the positioning of the camera are described along with discussion on the probable reason for the issue and the derived solution. Next, the development of the software to actuate the camera is explained. The implementation decisions are clarified, and example snippets are given to illustrate the usage of the created software. Finally, the algorithm implementation is described. The software developed to manipulate and interpret image data is depicted. Issues faced in the implementation process are explained along with the steps taken to rectify them.

5.1 Hardware Installation

The hardware was installed in the target environment as illustrated in Figure 7. Some time was spent finalizing the location and installation method of the camera. Initial location revealed issues related to the image capturing method. Figure 13 presents an intensity image of a scrap basket captured from the initial installation location. There is an obvious light band on the right side of the image. The image is also quite gray and hazy. This is a result of gamma correction performed on the intensity image. Without gamma correction, the image would be very dark. This was due to a vertical bar in the safety railing. The vertical railing was not in front of the camera, but close enough to cause a major disturbance in image capturing, likely due to it reflecting the radiation emitted by the camera. Consequently, the camera was moved a bit further away from the vertical bar in the railing. Figure 14 shows an image taken from the final camera location. The basket is now in full view and there are no anomalies present in the image.

Figure 13. Initial camera installation with a lighter band on the right side.

Figure 14. Image from the final camera position.

5.2 Image Capture Software Development

Software was written as designed in Figure 10 using Python programming language. The initial requirement was the ability to capture images using the camera. The *Harvesters* image acquisition library was used for this purpose. It implements the GenICam API to enable effortless image acquisition. "Harvesters simple use case" code snippet in Appendix A demonstrates a simple use case for the library.

First, we construct a Harvester object, which handles manufacturer descriptor files and keeps track of available devices. The descriptor file is added to the Harvester, after which the update method is called. This causes the Harvester to consume the provided descriptor files and attempts to find devices accordingly. The descriptor files contain the necessary implementations of the transport layer interface used by the camera. Next, an Image Acquirer (**ia** in the snippet) object is created using the Harvester. The individual cameras may be identified by their serial numbers, for example. The Image Acquirer object enables the configuration of individual cameras, as well as image capturing. The code snippet contains an example of image capturing.

The software used to operate the camera was developed to make use of the Harvesters library. The *cam* module of the *scrapvol* package contains two classes: CamReader and BlazeReader. CamReader is designed to abstract away all the Harvester related code, such as setting up and storing the Harvester object, creating Image Acquirers as necessary and handles image capturing. The design allows subclassing in a way that minimizes development time for using different GenICam compliant cameras. The BlazeReader is a subclass of the CamReader. It contains code specifically related to the Basler Blaze 101 camera. The BlazeReader class only implements camera configuration and feature manipulation as specified by the manufacturer. It also must specify the descriptor file consumed by Harvester. To enable quick configuration without the need for code changes, a configuration file is employed to enable users to set and control features of the camera, such as exposure time and whether certain filters are used. "BlazeReader simple use case" code snippet in Appendix A demonstrates creating a BlazeReader object and using it to capture a single point cloud. The returned point cloud is a PointCloud object created using the Open3D library. The Open3D library was selected because it contains numerous useful algorithms and functions for manipulating and visualizing point clouds. Furthermore, the library is fully open source and is developed by an active community. Further details on the library and its use later.

5.3 Algorithm Implementation

After the final position of the camera was established, a simple program was written to capture images of baskets whenever one arrived at the loading zone. Upon analyzing some images, it was determined that the camera exhibits some degree of variance in the absolute distance measurements. Originally, it was hypothesized that the distance measurements would be mostly consistent. This would allow a static transformation and subsequent static cropping of the point cloud to extract only pixels belonging to the basket or scrap surface. Due to variance in the absolute distance measurement, this approach would probably lead to erroneous results.
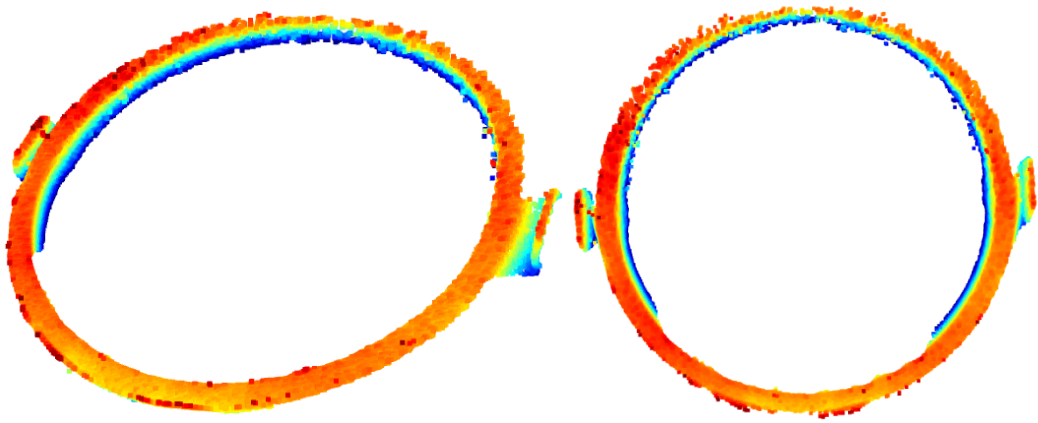
Therefore, another approach had to be devised. The solution was to use a reference point cloud to ensure consistency. Aligning subsequent point clouds with the reference point cloud allows the normalization of coordinates. The reference point cloud was carefully selected such that there is an abundance of basket top edge pixels present. Figure 15

presents the selected point cloud and Figure 16 presents the extracted basket top edge pixels. Finally, a coordinate transform was found manually for the point cloud containing just the basket top edge points, such that the z-axis is precisely (as close as possible) perpendicular to the scrap basket. Now, aligning new point clouds with this point cloud accomplishes three things. First, the distance to the basket top edge is known. Second, the z-value of scrap pixels directly relates to the depth of the scrap surface relative to the basket top edge. Third, because it is known where the basket top edge pixels are, the scrap surface pixels may be extracted. This is accomplished simply by cropping the point cloud according to the basket edge coordinates. At this point, the distance to the basket edge is known from the basket top edge reference point cloud. Furthermore, the distance to the scrap surface may be calculated by averaging the z-values of the scrap surface pixels. The scrap surface height relative to the basket may then be calculated using equation 4.

(a) Amplitude image   (b) Range image

(a) Point cloud (front view)   (a) Point cloud (right side view)
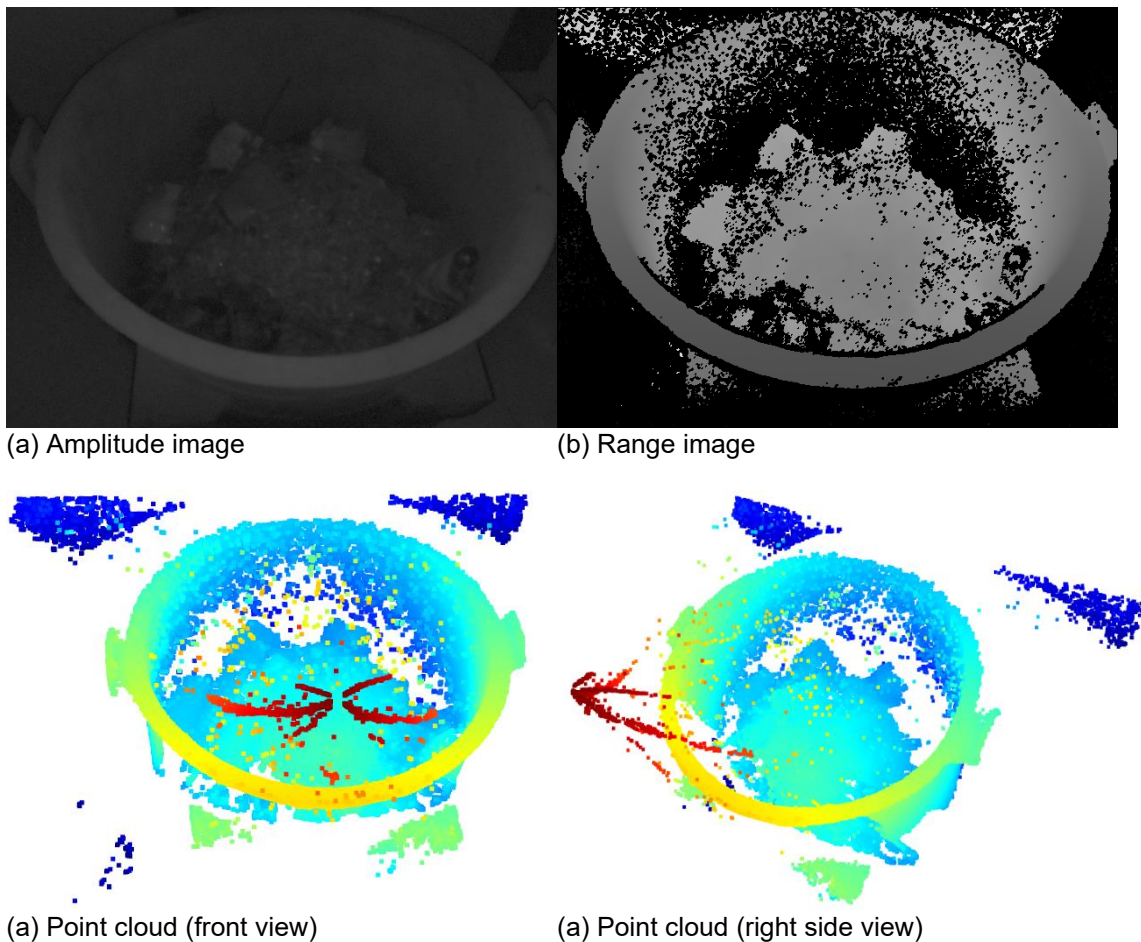
Figure 15. The selected reference point cloud.

Figure 16. Basket top edge points extracted from the reference point cloud.

From the point clouds it was quickly determined that some processing had to be conducted on the point clouds to enable analysis. First, the inbuilt camera features were utilized to remove as much of the erroneous measurements as possible while maintaining the maximum number of valid measurements. Each of the image quality features that were enumerated before were utilized. The threshold or strength values for each feature were experimentally determined to obtain the best possible images. However, the resulting measurements still contained disturbances. To further improve image quality, an additional statistical outlier removal method presented by Rusu et al. (2008b) was used. Figure 17 illustrates the effectiveness of the method.
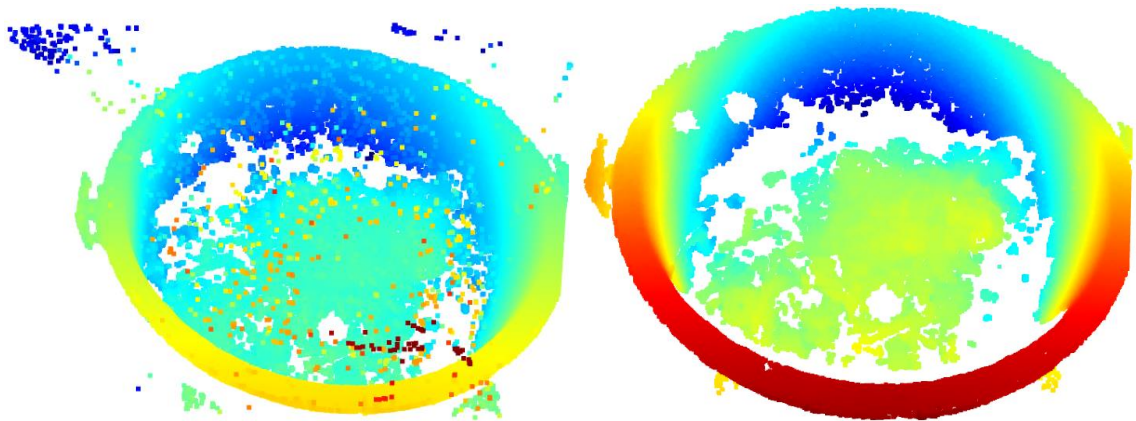
Figure 17. Point cloud outlier removal. Left image: original point cloud. Right image: point cloud after outlier removal.

Software implementation of the algorithm employed the Open3D image processing library. The *pcdfun*, *pcdalign*, and *pcddisp* modules were developed. The *pcdfun* module contains generic point cloud functions that allow processing the point clouds. These include rotating, cropping, removing outliers, and creating PointCloud objects from coordinates. The *pcddisp* module contains functions that allow visualizing point clouds. Finally, *pcdalign* contains the functions related to aligning point clouds with each other.

As noted, the Open3D library was used as it implements many algorithms and other functionality related to manipulating and processing point clouds. The most important object defined in the library is the PointCloud object, which in itself contains numerous helpful methods to manipulate point clouds. Furthermore, many of the functions defined in the library accept PointCloud objects as inputs. Therefore, the first objective of the software was to construct a PointCloud object from the captured depth data. This was

quite simple to achieve, as the coordinate data provided by the Basler Blaze-101 camera could be directly used as input to the PointCloud construction function.

Upon constructing the PointCloud object, implementing the scrap volume algorithm was effortless. Outliers are removed using the PointCloud object's statistical outlier removal method, which uses the algorithm presented by Rusu et al. (2008b). The next stage of the algorithm is aligning point cloud with the basket top edge reference point cloud. Open3D conveniently implements geometric feature finding, rough registration, and fine registration methods. First, the point clouds are down sampled using voxel down sampling. A voxel grid is a uniform 3D grid, where each pixel belongs to precisely one voxel. For each voxel, a single point is generated by averaging the contained points. The size of the voxel determines the degree of down sampling.

Next, for both point clouds, surface normals are estimated. This is required by the function that computes the FPFH features presented by Rusu et al. (2009). Finally, the rough registration is computed using the fast global registration by Zhou et al. (2016). The result of the rough transformation is used as input to the fine registration method. The fine registration method is the ICP algorithm. The transformation that aligns the point cloud with the basket top edge reference point cloud is performed using the rotate method of the PointCloud object. The final step is extracting the scrap surface points by cropping the point cloud according to the known basket edge points. Finally, the scrap surface level height relative to the scrap basket is calculated using equation 4.

6.   Evaluation

This chapter covers the usage of the complete scrap volume measurement system. As explained in the research method chapter, the applicability of the system is demonstrated in the target environment. Upon starting the system, the camera is configured according to the configuration file. The system then waits for a signal from the automation system until a scrap basket is in place to be imaged. When a basket arrives, the system operates the camera to obtain a depth image of the basket, along with an intensity image and a data array of (x, y, z) coordinates. The system then proceeds to compute the fill percentage of the basket as explained before. Finally, the result is broadcasted to whichever system is interested in receiving it.

Figure 18 presents the intensity and depth images of a scrap basket, thus demonstrating that the system can receive a signal from the automation system, as well as capturing depth images using the camera. The image quality looks acceptable. Figure 19 presents the pre-processed point cloud, and a combined point cloud with the basket top edge reference point cloud. It is evident from the image that plenty of basket top edge pixels were obtained. Moreover, many scrap surface pixels were obtained, even though some were invalidated. It is noteworthy, however, that some of the white pixels in the image are simply not visible to the camera. Those are the pixels that lie behind the scrap pile.
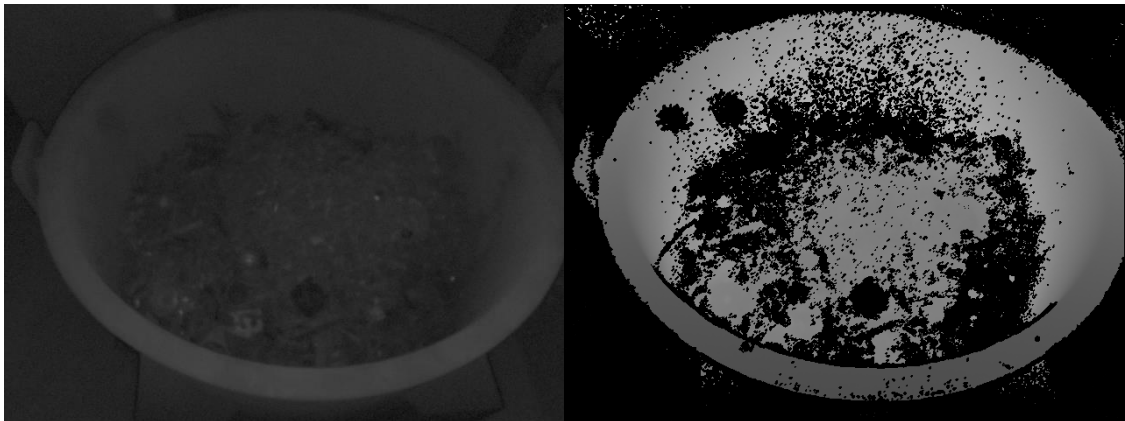

Figure 18. The scrap basket intensity (left) and depth (right) images.
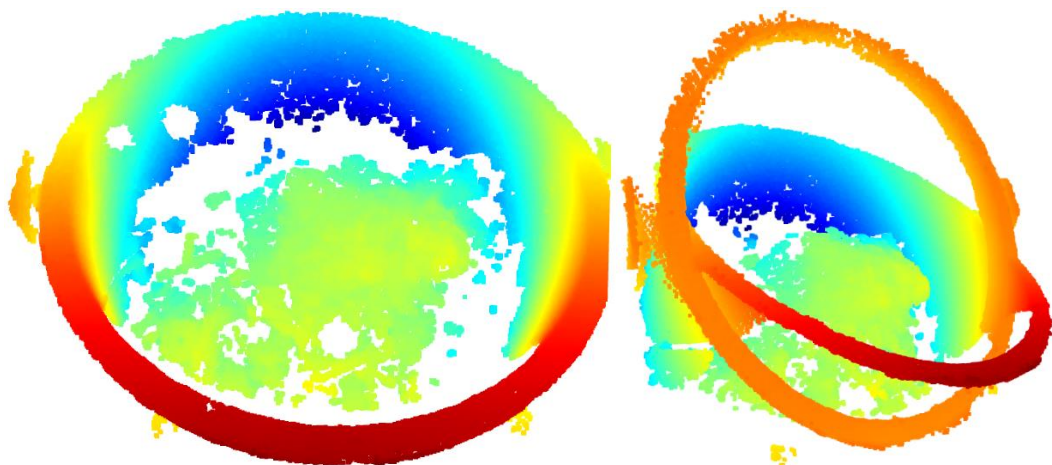
Figure 19. The pre-processed point cloud (left). The right image also visualizes the basket top edge reference point cloud.

The basket fill percentage may now be computed. First the point cloud is aligned with the reference point cloud. Figure 20 presents the results of the rough and fine registration results. Looking at the images, the rough transformation does a pretty good job with aligning the point clouds. However, the fine registration does seem necessary and based on the image it does accomplish an acceptable alignment. Table 1 presents the registration results. The fitness value describes the successfulness of the registration, with a value of 1.0 denoting perfect registration. Root-mean-square error (RMSE) describes how erroneous the registration turned out, with a value of 0.0 meaning no error. From the table, it is evident that the fine registration improved the registration. In addition to fitness and RMSE, the number of points in the point cloud and the mean nearest neighbour distance were used to evaluate the final registration. The nearest neighbour distance is the distance from a point on the reference point cloud to the nearest point on the aligned point cloud. This property proved useful in cases where a captured point cloud was lacking in basket edge points. As may be observed in Figure 20, the reference point cloud contains only the basket edge, whereas the aligned point cloud also contains points belonging to the scrap surface. This explains the seemingly low fitness and large RMSE values. Success criteria for these were experimentally determined and are shown in the final row of Table 1.
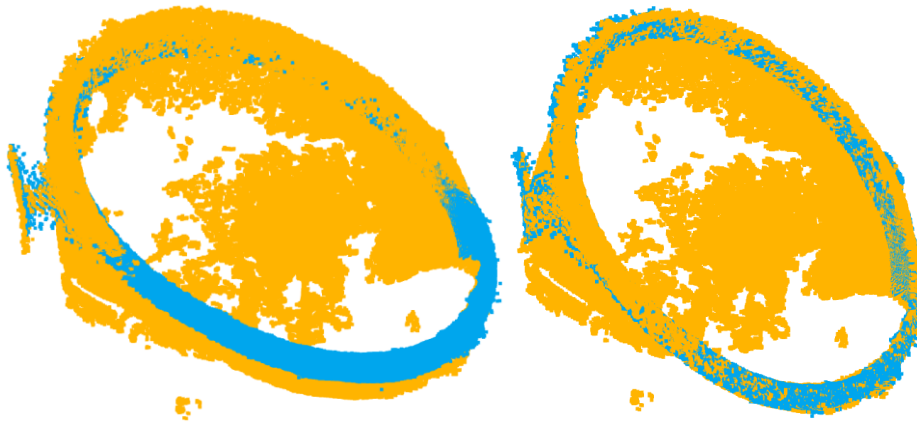

Figure 20. Rough (left) and fine (right) registration results. Blue pixels belong to the reference point cloud and orange pixels to the image to be aligned.

Table 1. Registration results.

Registration	Fitness	RMSE	Mean nearest neighbour distance	# Points
Rough	0.271	48.08		
Fine	0.437	26.56	14.56 mm	134 057
Success criteria	> 0.40	< 40.00	< 400 mm	> 30 000

Figure 21 presents the point cloud transformed according to the fine registration result. Red colour corresponds to pixels that are closest and blue colour to the farthest pixels. Observing the top edge of the basket visually, it does look like the transformation result is acceptable. The top-most points of the basket edge are all a dark red colour, relating to the closest points, and the lowest points blue, corresponding to the farthest points.
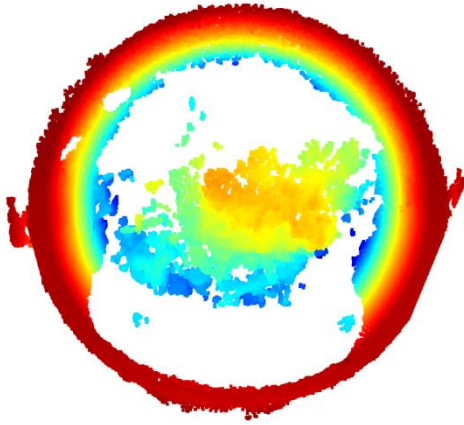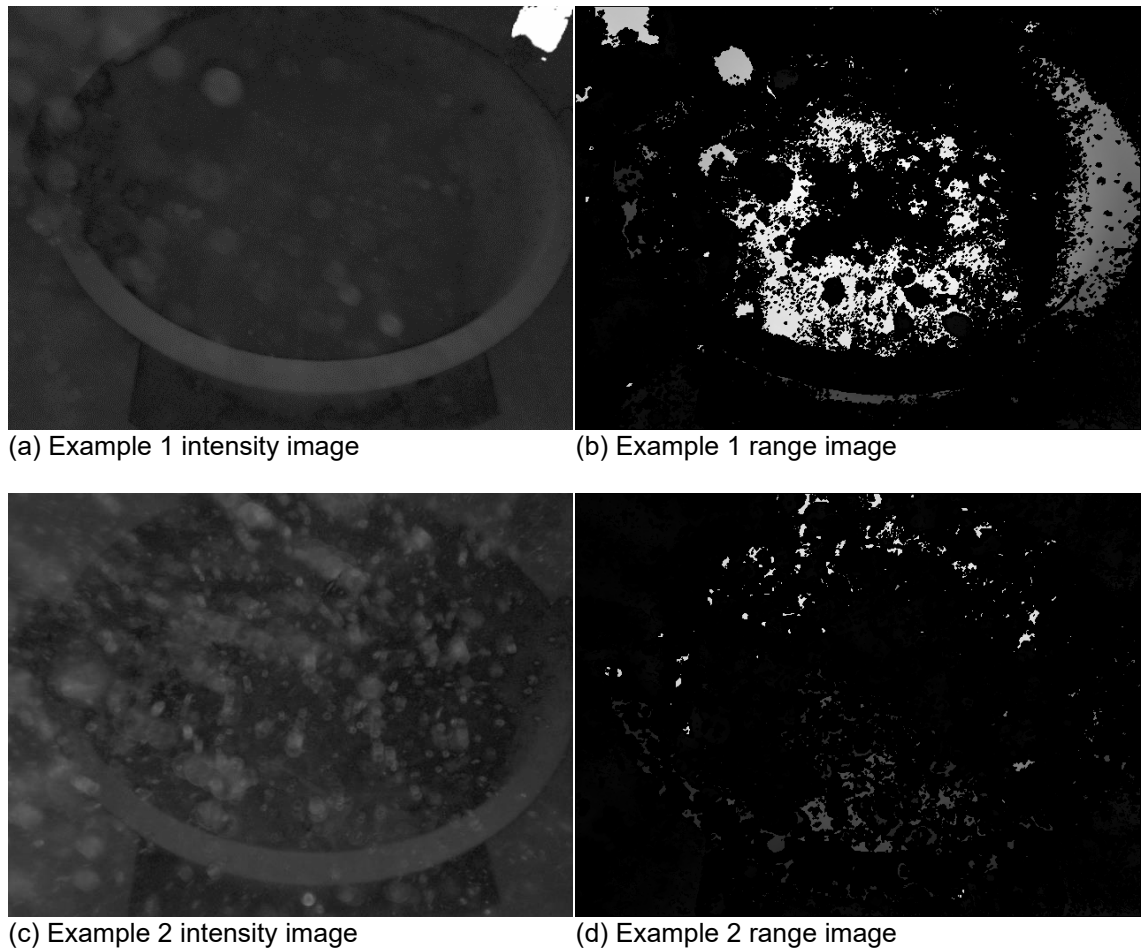
Figure 21. Point cloud transformed according to the fine registration result.

Finally, Figure 22 presents the scrap surface extracted from the transformed point cloud. The scrap surface point cloud contains 37 061 points. Visual evaluation suggests that the system was able to extract the points related to the scrap surface. Thereafter, the average of the z-values of the scrap surface pixels is easily obtained. The result is that the depth of the scrap surface with respect to the basket top edge is 1.19 meters. Using knowledge of the basket height, the system can compute the basket fill percentage, which is directly related to the scrap volume in the basket. Relating this to the intensity image presented in Figure 18, the result is plausible. It has therefore been shown that the system can complete the task it was designed for. Unfortunately, more accurate evaluation of the result is difficult, as the true volume of the scrap is unknown. Another example of the algorithm result is included in Appendix B.
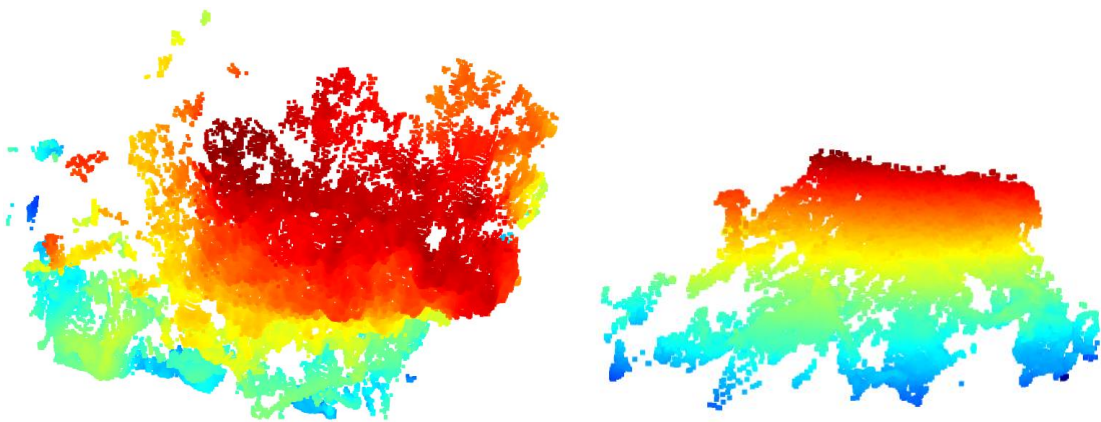
Figure 22. Point clouds of the extracted scrap surface. Left is view from above and right is view from the side.

In some cases, image capturing was unsuccessful. The most noteworthy failure cases resulted from either a dust cloud in front of the camera or very dark metal scrap. The steel factory as an environment is difficult because of steel dust floating in the atmosphere. Different steel scrap materials have different chemical compositions. The steel scrap is layered into the baskets in a precalculated manner according to the desired steel grade of the final product. The reflectiveness of the scrap varies greatly.

(a) Example 1 intensity image   (b) Example 1 range image

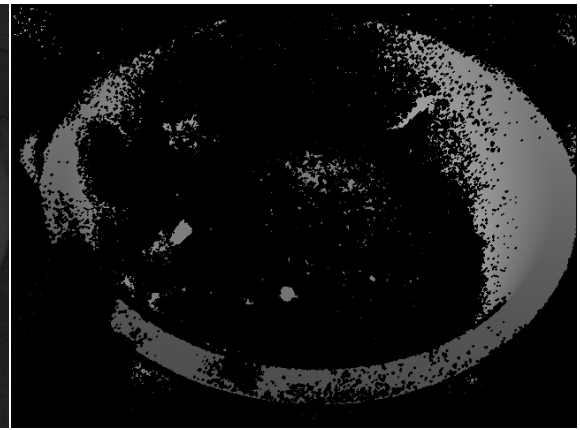(c) Example 2 intensity image   (d) Example 2 range image

Figure 23. Poor-quality images resulting from dust in front of the camera and their respective depth images.

It is inevitable that sometimes a cloud of steel dust will block the view of the camera. Figure 23 presents two examples of poor-quality images resulting from a dust cloud in view of the camera. A simple solution to avoid this issue is to examine the registration results and capturing a new image when success criteria are not met. Another possible solution could be to capture multiple images with a set interval between subsequent shots and constructing a clearer image from them. Mitigating this issue is not in the scope of this thesis, however. The problem could be explored in a later study.

Figure 24 presents the other notable failure case resulting from the imaging target being particularly dark and unreflective. This situation is more difficult than the steel dust case. The root cause is that the camera is unable to measure distance to the target due to hardly any light reflecting from the target. Thus, the camera is unable to determine the phase difference required to compute the corresponding distance to the target. It is difficult to say at this point how the problem could be mitigated. Again, further research could be conducted to tackle this issue.
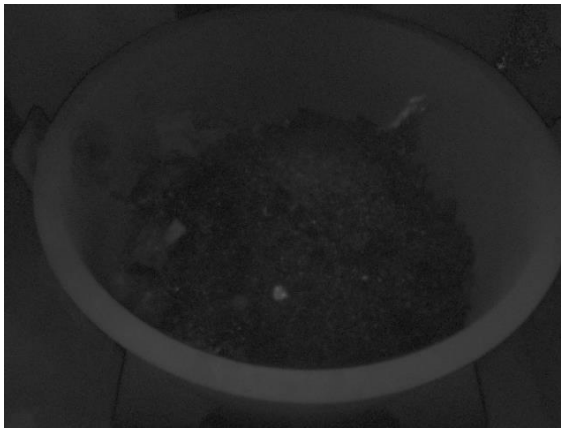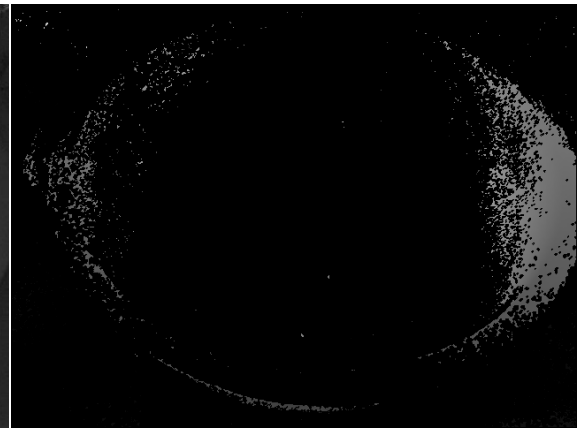
(a) Example 1 intensity image

(b) Example 1 range image

(c) Example 2 intensity image

(c) Example 2 range image

Figure 24. Poor quality images resulting from very dark and unreflecting scrap.

7.   Discussion

An algorithm to compute the fill percentage of scrap baskets was successfully developed. Furthermore, the ability of the artifact to compute the scrap basket fill percentage was demonstrated successfully in the target industrial context. Assuming that there are no external factors that might influence the image quality, the algorithm performs adequately well. Image acquisition normally takes less than one second. The processing time of the point cloud is in the order of seconds, which could probably be reduced by decreasing the computational complexity by down sampling the processed point clouds, for example.

The camera hardware performed sufficiently well. After the installation location of the camera was finalized, there were no more static issues with image capturing. The more pressing matters associated with capturing images are the issues related to the ambient dust clouds moving around in the factory atmosphere as well as the reflectivity (or lack thereof) of some scrap grades. To some degree, these issues were mitigated by recapturing the image if the image registration did not meet success criteria. This solution has some problems. First, the scrap basket may not be in view of the camera anymore when the new image would be captured. That is, the operators might lift the basket before a new image could be captured, resulting in an empty image. Second, it does not address the root issues, but naïvely assumes that the second image will turn out better than the first. Now, sometimes that was indeed the case. The dust cloud could have passed between capturing the images. However, capturing a new image of unreflective material does not lead to a better result.

Attempts were made to improve image quality by adjusting the internal camera settings and features. The varying reflectivity of different scrap grades provides a challenge to image acquisition, especially when determining the used exposure time. Some scrap pieces may be highly reflective, necessitating the use of a shorter exposure time to avoid oversaturation. Other types of scrap may be the complete opposite, requiring a longer exposure time to obtain measurements. It was noted based on some experimentation that the maximum exposure time allowed by the camera yielded the best results. The filter features of the camera were all employed and the threshold or strength values for each were determined separately. It was noted that each filter improved the image quality. However, the process for selecting the threshold or strength values could have been carried out in a more rigorous manner.

There is also an issue related to the algorithm itself. Since a reference image is required to execute the coordinate transformation reliably, setting up the algorithm requires some manual configuration, testing and estimation. The reference image must be selected, the basket edge pixels and the corresponding cropping values must be found manually, and the rotation parameters must be determined. These steps must be taken for each camera separately. Furthermore, if the camera location must be changed, these steps must be redone. Arguably, however, the magnitude of these efforts is negligible compared to the potential benefits of the system.

Further research should be conducted to address the issues outlined above. It is possible that the scrap surface could be found programmatically without the use of a reference image. Finding the pixels in point clouds that belong only on the scrap surface or the basket would eliminate the need for a reference image. Removing the need for a reference image also indirectly reduces the computational complexity of the algorithm. It is not certain, however, that employing a different method for finding the scrap surface would reduce computation time. Furthermore, some method for determining the quality of the

image immediately after capturing would enable rejecting unusable images in an earlier stage in the procedure. Such cases are, for example, the presence of a dust cloud blocking the view of the camera or unreflective scrap causing hardly any pixels to be acquired of the scrap surface. Determining the quality of the captured image is only half of a solution. The other half is how to mitigate the effect of the mentioned phenomena.

Cameras from different manufacturers should be considered for possible performance gains. A technology called High Dynamic Range (HDR) is a noteworthy technology that is based on capturing multiple images of the scene using different exposure times. This enables capturing high quality images of scenes with varying reflectivity. Some cameras implement this technology on the camera hardware, which is significantly faster than a pure software implementation.

Ultimately, the system is intended to be used in conjunction with the Luxmet ArcSpec system to accurately time scrap basket charging into electric arc furnaces. This study demonstrates the feasibility of acquiring the volume of the charged scrap. Further research should be conducted to combine this information with the data produced by the ArcSpec system, as well as other process parameters to achieve more accurate charging timing.

8.   Conclusion

Energy efficiency, emissions and sustainability are major trends in the steel industry. The demand for steel is projected to grow in the coming decades, while at the same time emissions should be reduced drastically. Therefore, all feasible methods to improve the energy efficiency of steel making should be considered. One solution is to transition from static control of the process more and more towards dynamic methods. Determining the timing of the charging of scrap baskets dynamically is one of many of such methods.

The objective of this study was to develop a system which would help in facilitating dynamic charging timing by providing accurate information of scrap volume in charging baskets. The purpose is to avoid problems caused by early charging and reduce the adverse effect on energy efficiency caused by late charging. Accurate timing of charging is possible with information on the volume of scrap being charged and the free volume inside the furnace.

Depth imaging hardware was used in the thesis to measure 3D data of scrap baskets. A camera was installed in the production environment in the melting shop of a steel factory. Software was developed to configure and actuate the camera. The camera features were experimented with, and suitable parameters were determined to obtain good quality images. An algorithm was subsequently developed and implemented in software to find the points belonging to the basket, as well as the scrap surface from the data. These points were then used to calculate the depth of the scrap surface relative to the basket top edge. Finally, knowledge of the basket dimensions could be used to compute the volume of metal scrap inside the basket.

It was demonstrated that information of the scrap volume may be obtained using depth imaging and the algorithm developed in this thesis. Feasible results were obtained in cases where the depth image quality was sufficient. Most notable issues related to obtaining depth images were dust clouds inherent to melt shops and the low reflectivity of some scrap grades.

Further research should be conducted to further evaluate the accuracy of the measurements. Moreover, technological innovations such as HDR and other camera hardware features should be explored to achieve better quality depth images specifically in this context. Furthermore, the computational complexity of the algorithm and ways to improve it should be examined. Finally, the information on the melting stage inside the furnace provided by Luxmet ArcSpec system should be combined with the scrap volume data to achieve an accurate timing of scrap basket charging.

References

Axelsson, P. (1999). Processing of laser scanner data - algorithms and applications. *ISPRS Journal of Photogrammetry and Remote Sensing*, *54*(2-3), 138-147.

Basler. (2022). Basler Product Documentation. Available online: https://docs.baslerweb.com/blaze-101 (accessed on 5 October 2022).

Besl, P. J. (1988). Active optical range imaging sensors. *Advances in machine vision*, 28(1), 127-152.

Besl, P. J., & McKay, N. D. (1992). Method for registration of 3-D shapes. In *Sensor fusion IV: control paradigms and data structures* (Vol. 1611, pp. 586-606). Spie.

Blais, F. (2004). Review of 20 years of range sensor development. *Journal of Electronic Imaging*, 13(1), 231-240.

Breunig, M. M., Kriegel, H. P., Ng, R. T., & Sander, J. (2000). LOF: identifying density-based local outliers. In *Proceedings of the 2000 ACM SIGMOD international conference on Management of data* (pp. 93-104).

Chen, F., Brown, G. M., & Song, M. (2000) Overview of three-dimensional shape measurement using optical methods. *Optical Engineering*. 39(1).

Chen, Y., & Medioni, G. (1992). Object modelling by registration of multiple range images. *Image and vision computing*, *10*(3), 145-155.

Cohen, Y., Faccio, M., Pilati, F., Yao, X. (2019). Design and management of digital manufacturing and assembly systems in the Industry 4.0 era. *The International Journal of Advanced Manufacturing Technology*, *105*(9), 3565-3577.

Han, X. F., Jin, J. S., Wang, M. J., Jiang, W., Gao, L., & Xiao, L. (2017). A review of algorithms for filtering the 3D point cloud. *Signal Processing: Image Communication*, *57*, 103-112.

Hansard, M., Lee, S., Choi, O. & Horaud, R. (2013). *Time-of-Flight Cameras: Principles, Methods and Applications* (1st ed. 2013.). Springer London.

Hao, R., Lu, B., Cheng, Y., Li, X., & Huang, B. (2021). A steel surface defect inspection approach towards smart industrial monitoring. *Journal of Intelligent Manufacturing*, *32*(7), 1833-1843.

Hevner, A. R., March, S. T., Park, J., & Ram, S. (2004). Design science in information systems research. *MIS Quarterly: Management Information Systems*, 28(1).

Holappa, L. (2020). A general vision for reduction of energy consumption and CO_2 emissions from the steel industry. *Metals*, *10*(9), 1117.

Horaud, R., Hansard, M., Evangelidis, & G., Ménier, C. (2016). An Overview of Depth Cameras and Range Scanners Based on Time-of-Flight Technologies. *Machine Vision and Applications*, 27(7).

Hsu, C. Y., Lin, H. Y., Kang, L. W., Weng, M. F., Chang, C. M., & You, T. Y. (2017). 3D modeling for steel billet images. In *2017 IEEE International Conference on Consumer Electronics-Taiwan (ICCE-TW)* (pp. 5-6). IEEE.

Jarvis, R. A. (1983). A Perspective on Range Finding Techniques for Computer Vision. *IEEE Transactions on Pattern Analysis and Machine Intelligence*, PAMI-5(2).

Jones, J.A.T., Bowman, B. & Lefrank, P.A. (1998). Electric Furnace Steelmaking. In R.J. Fruehan (Ed), *The Making, Shaping and Treating of Steel* (pp. 525-660). Pittsburgh, USA: The AISE Steel Foundation. ISBN 0-930767-02-0.

Knorr, E. M., & Ng, R. T. (1998). Algorithms for mining distance-based outliers in large datasets. In *Proceedings of the international conference on very large data bases* (pp. 392-403). Citeseer.

Landström, A., & Thurley, M. J. (2012). Morphology-based crack detection for steel slabs. *IEEE Journal of selected topics in signal processing*, *6*(7), 866-875.

Lefloch, D., Nair, R., Lenzen, F., Schäfer, H., Streeter, L., Cree, M. J., Koch, R., & Kolb, A. (2013). Technical foundation and calibration methods for time-of-flight cameras. In *Time-of-Flight and Depth Imaging. Sensors, Algorithms, and Applications* (pp. 3-24). Springer, Berlin, Heidelberg.

Neogi, N., Mohanta, D. K., & Dutta, P. K. (2014). Review of vision-based steel surface inspection systems. *EURASIP Journal on Image and Video Processing*, *2014*(1), 1-19.

Nurunnabi, A., West, G., & Belton, D. (2015). Outlier detection and robust normal-curvature estimation in mobile laser scanning 3D point cloud data. *Pattern Recognition*, *48*(4), 1404-1419.

Park, C., Bae, H., Yun, J., & Yun, S. (2013). The automated surface inspection system for hot slab. In *2013 13th International Conference on Control, Automation and Systems (ICCAS 2013)* (pp. 1733-1735). IEEE.

Peffers, K., Tuunanen, T., Rothenberger, M. A., & Chatterjee, S. (2007). A design science research methodology for information systems research. *Journal of management information systems*, 24(3), 45-77.

Rusinkiewicz, S., & Levoy, M. (2001). Efficient variants of the ICP algorithm. In *Proceedings third international conference on 3-D digital imaging and modeling* (pp. 145-152). IEEE.

Rusu, R. B., Blodow, N., Marton, Z. C., & Beetz, M. (2008a). Aligning point cloud views using persistent feature histograms. In *2008 IEEE/RSJ international conference on intelligent robots and systems* (pp. 3384-3391). IEEE.

Rusu, R. B., Marton, Z. C., Blodow, N., Dolha, M., & Beetz, M. (2008b). Towards 3D point cloud based object maps for household environments. *Robotics and Autonomous Systems*, *56*(11), 927-941.

Rusu, R. B., Blodow, N., & Beetz, M. (2009). Fast point feature histograms (FPFH) for 3D registration. In *2009 IEEE international conference on robotics and automation* (pp. 3212-3217). IEEE.

Sansoni, G., Trebeschi, M., Docchio, F. (2009). State-of-the-art and applications of 3D imaging sensors in industry, cultural heritage, medicine, and criminal investigation. *Sensors*. 9(1).

Sugiyama, M., & Borgwardt, K. (2013). Rapid distance-based outlier detection via sampling. *Advances in neural information processing systems*, *26*.

World Steel Association. (2021a). Policy paper: climate change and the production of iron and steel. Available online: https://worldsteel.org/publications/bookshop/climate-change-and-the-production-of-iron-and-steel/ (accessed on 1 September 2022).

World Steel Association. (2021b). Sustainability Indicators 2021 and our sustainability journey. Available online: https://worldsteel.org/publications/bookshop/sust2021/ (accessed on 1 September 2022).

World Steel Association. (2022) World Steel in Figures 2022. Available online: https://worldsteel.org/steel-topics/statistics/world-steel-in-figures-2022/ (accessed on 1 September 2022).

Zanuttigh, P., Marin, G., Dal Mutto, C., Dominio, F., Minto, L. & Cortelazzo, G. M. (2016). *Time-of-Flight and Structured Light Depth Cameras: Technology and Applications* (1st ed. 2016.). Springer International Publishing.

Zhao, L. M., Ouyang, Q., Chen, D. F., & Wen, L. Y. (2011). Surface defects inspection method in hot slab continuous casting process. *Ironmaking & Steelmaking*, *38*(6), 464-470.

Appendix A

Harvesters simple use case:

```
from harvesters.core import Harvester
import numpy as np
h = Harvester()
h.add_file("path/to/basler_blaze_description_file")
h.update()
ia = h.create(0)
ia.start()
with ia.fetch() as buff:
        component = buff.payload.components[0]
        height = component.height
        width = component.width
        raw_image = np.copy(component.data)
ia.stop()
```
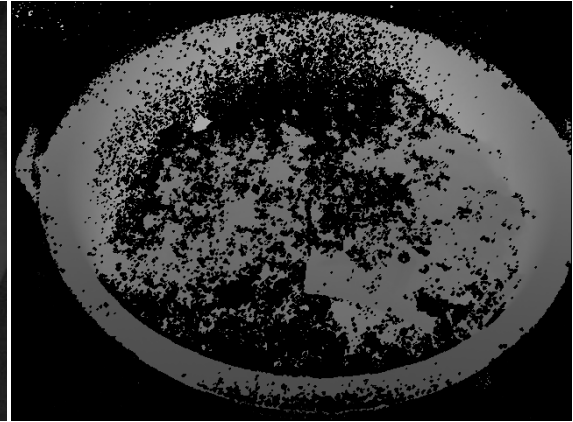
BlazeReader simple use case:

```
from configparser import ConfigParser
from scrapvol.cam import BlazeReader
config = ConfigParser()
config.read("blaze_config.ini")
reader = BlazeReader.from_config(config["cam1"])
point_cloud = reader.capture_pcd()
```

Appendix B

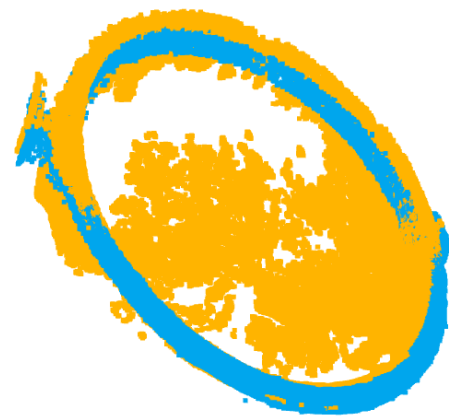Example of the algorithm.

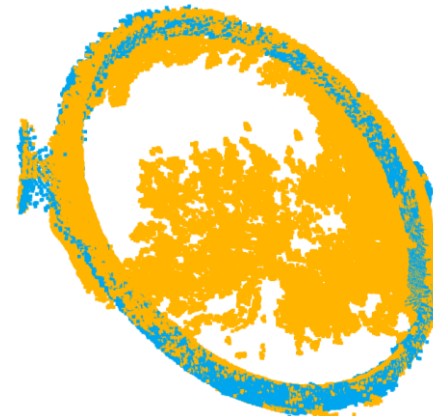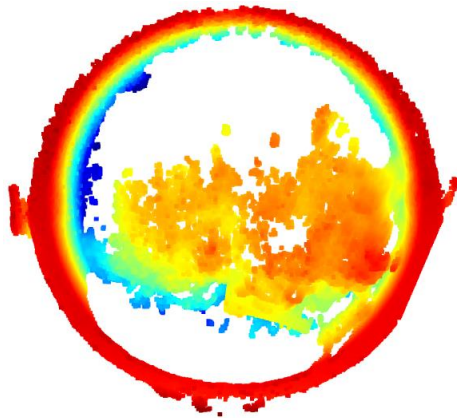(a) Intensity image

(b) Range image
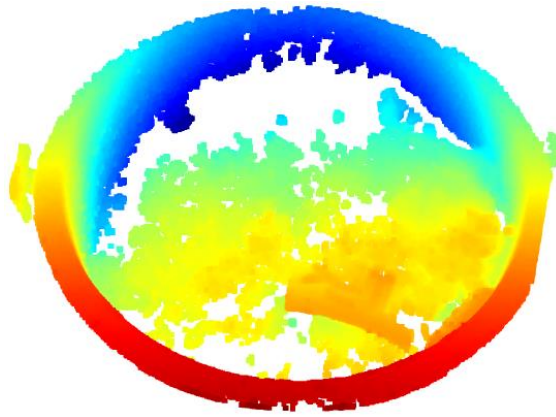
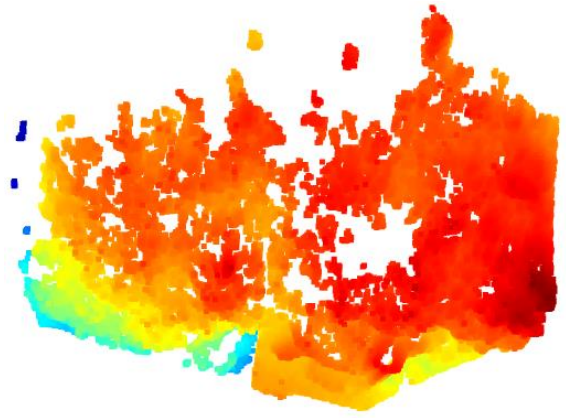

(c) Point cloud
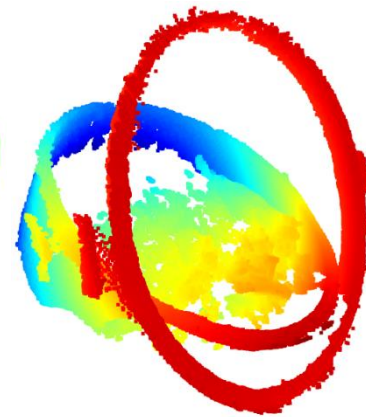
(d) Point cloud with reference

(e) Rough registration result

(f) Fine registration result

(g) Transformed point cloud

(h) Scrap surface point cloud

Registration	Fitness	RMSE	Mean nearest neighbour distance	# Points
Rough	0.387	59.14		
Fine	0.430	25.85	15.00 mm	129 268
Success criteria	> 0.40	< 40.00	< 400 mm	> 30 000

FINAL RESULT: Scrap surface is 0.50m below the basket top edge.